High spatial resolution mapping and source-apportionment of aerosol composition ~~and sources~~ in Oakland, California using mobile aerosol mass spectrometry

Rishabh U. Shah[1,2], Ellis S. Robinson[1,2], Peishi Gu[1,2], Allen L. Robinson[1,2], Joshua S. Apte[3], and Albert A. Presto[1,2]

[1]Mechanical Engineering, Carnegie Mellon University, Pittsburgh PA
[2]Center for Atmospheric Particle Studies, Carnegie Mellon University, Pittsburgh PA
[3]Department of Civil, Architectural and Environmental Engineering, University of Texas at Austin, Austin TX

Correspondence: Albert A. Presto (apresto@andrew.cmu.edu)

Abstract. We investigated spatial and temporal patterns in concentration and composition of sub-micron particulate matter (PM_1) in Oakland, California in the summer of 2017 using an aerosol mass spectrometer mounted in a mobile laboratory. We performed $\sim$ 160 hours of mobile sampling in the city over a 20-day period. Measurements are compared for three adjacent neighborhoods with distinct land uses: a central business district ("downtown"), a residential district ("West Oakland"), and a major shipping port. The average organic aerosol (OA) concentration is 5.3 μ~~gm~~g m^{-3} and contributes $\sim$ 50% of the PM_1 mass. OA concentrations in downtown are, on average, 1.5 μ~~gm~~g m^{-3} higher than in West Oakland and Port. We decomposed OA into three factors using positive matrix factorization: hydrocarbon-like OA (HOA; 20% average contribution), cooking OA (COA; 25%) and ~~semi-volatile oxidized OA (SV-OOA~~less-oxidized oxygenated OA (LO-OOA; 55%). The collective 45% contribution from primary OA (HOA + COA) emphasizes the importance of primary emissions in Oakland. The dominant source of primary OA shifts from HOA-rich in the morning to COA-rich after lunch time. COA in downtown is consistently higher than West Oakland and Port due to a large number of restaurants. HOA exhibits variability in space and time. Morning-time HOA concentration in downtown is twice that in Port, but Port HOA increases more than two-fold during mid-day, likely because trucking activity at the Port peaks at that time. Combining measurements of OA with black carbon and CO suggests that while trucks have an important effect on OA and BC at the Port, gasoline-engine cars are the dominant source of traffic emissions in the rest of Oakland. Despite the expectation of being spatially uniform, ~~SV-OOA~~ LO-OOA also exhibits spatial differences. Morning-time ~~SV-OOA~~ LO-OOA in downtown is roughly 25% ($\sim$ 0.6 μ~~gm~~g m^{-3}) higher than the rest of Oakland. Even as the entire domain approaches a more uniform ~~photo-chemical~~ photochemical state in the afternoon, downtown ~~SV-OOA~~ LO-OOA remains statistically higher than West Oakland and Port, suggesting that downtown is a microenvironment with higher photochemical activity. Higher concentrations of particulate sulfate (also of secondary origin) with no direct sources in Oakland further reflect higher photochemical activity in downtown. A combination of several factors (poor ventilation of air masses in street canyons, higher concentrations of precursor gases, higher concentrations of the hydroxyl radical) likely result in the proposed high photochemical activity in downtown. Lastly, through Van Krevelen analysis of elemental ratios (H/C, O/C) of the OA, we show that OA in Oakland is more chemically reduced than several other urban areas. This underscores the

importance of primary emissions in Oakland. We also show that mixing of oceanic air masses with these primary emissions in Oakland is an important processing mechanism that governs the overall OA composition in Oakland. ~~The findings of this study are important because the pollutants we find contributing the most to OA variability, both of primary and secondary origin, are ubiquitous in other urban locations.~~

1 Introduction

Organic aerosol (OA) contributes a significant fraction of the total ambient particulate matter (PM) mass (Zhang et al., 2007), which is of utmost concern for its detrimental effects on human health (Apte et al., 2015) and the Earth's radiative budget (Myhre et al., 2013). However, owing to the tens of thousands of different emitted organic species and their chemical and physical transformation in the atmosphere, the concentration and composition of OA remains complex to characterize (Hallquist et al., 2009; Jimenez et al., 2009; Tsigaridis et al., 2006; Goldstein and Galbally, 2007).

Concentrations of PM and other pollutants are spatially variable in urban areas and these spatial variations drive differences in human exposures. For example, concentrations of ultrafine particles, NO, CO, and particulate black carbon (BC) are enhanced near highways by a factor of 2-3 relative to areas > 100m from roadways (Choi et al., 2012; Apte et al., 2017; Saha et al., 2018a). Spatial variations in PM mass are more modest (e.g., only a $\sim$ 25% increase near roadways; Saha et al., 2018a), but are convolved with significant variations in composition (Mohr et al., 2015; Enroth et al., 2016; Canagaratna et al., 2010). In the near-source region fresh emissions of BC and primary OA rapidly mix with background air, reducing concentrations through both dilution and OA partitioning. This rapid mixing occurs over ~~the space of~~ tens to hundreds of meters ~~and is expected to require timescales of minutes to hours (?)~~downwind of the source (Canagaratna et al., 2010; Saha et al., 2018a).

Studying these intra-urban PM variations can reveal the major sources influencing local air quality and help inform mitigation strategies. In particular, mobile sampling enables deployment of high-time-resolution measurements that can identify specific PM sources. For example, Li et al. (2018) showed that emissions of primary OA and BC drive much of the spatial variation in $PM_{2.5}$ observed in Pittsburgh. Apte et al. (2017) used mobile BC measurements to identify hotspots associated with vehicle traffic and industrial activities. Some studies have deployed aerosol mass spectrometers (AMS) on mobile platforms (Mohr et al., 2015; Elser et al., 2016; Von Der Weiden-Reinmüller et al., 2014). Factor analysis of AMS data allows for identification of chemically-specific OA sources, such as traffic, restaurant cooking, and home heating. For instance, Elser et al. (2016) found enhancements of hydrocarbon-like OA (HOA, from traffic emissions) and BC on busy roads during times of peak traffic and that traffic emissions were the dominant contributor to the urban increments of $PM_{2.5}$. In addition to traffic emissions, ~~Mohr et al. (2015) found~~ cooking and biomass burning emissions have also been shown to be prominent contributors to primary OA in ~~Barcelona~~urban areas (Mohr et al., 2015; Crippa et al., 2013b).

Quantifying PM and OA spatial gradients in urban areas, and identifying the sources driving those gradients, is important because more than half of the world's population lives in urban areas (United Nations, 2014). Large populations may therefore live or work in areas with elevated emissions and/or high OA concentrations. Identifying such areas, and the sources driving elevated concentrations, has far-reaching implications for both reducing human PM exposures and addressing socio-economic disparity in exposure to pollution on an intra-city scale.

This study presents results of mobile measurements conducted in Oakland, California. Oakland is a densely populated ($\sim$ 2900 inhabitants km^{-2}) pollution-source-rich city. It has a poverty rate (fraction of population below poverty line) of 18.9%, roughly twice as much as that of the collective San Francisco (SF) Bay area (9.2%) (US Census, 2016). It therefore offers a good test case for investigating spatial variations in OA, how these variations are influenced by high industrial presence in residential areas, and how these variations overlay with population. Oakland has a unique land-use feature in that a 1 km^2 downtown, a 6 km^2 mixed industrial and residential district, and one of the largest US shipping ports (5 km^2) all lie within a short spatial transect of 4 km (Figure 1A).

Several prior studies have focused on air quality in Oakland because of the influence of ships and associated drayage trucks (trucks that transport cargo between the port and ~~associated trucking activity~~ warehouses) driving through the residential district. Fisher et al. (2006) was one of the earlier studies addressing the heavy-duty diesel drayage trucks in Oakland as a mobile source. Since then, several legislations, such as enforcement of diesel particulate filters in drayage truck exhausts (CARB, 2011), improved truck queuing system to reduce idling (Giuliano and O'Brien, 2007), usage of low-sulfur fuel in ships approaching the port (CARB, 2009), and keeping shipping logistics gates open in the evening to dilute daytime congestion of drayage trucks (Port of Oakland, 2016) have been imposed to reduce port emissions and to improve Oakland's air quality. Consequently, recent studies have found substantial reductions in emissions from both drayage trucks and ships in Oakland (Preble et al., 2015; Dallmann et al., 2011; Tao et al., 2013). However, the presence of a large port and high drayage truck activity is still a large area source adjacent to the predominantly residential West Oakland district. Additionally, on the other side of this residential district lies downtown Oakland, which contains a mix of common urban emission sources (e.g., vehicular traffic emissions). Four interstate highways (I-80 and its arteries I-580, I-880, I-980) closely flank the residential district such that the largest spatial lag from any point inside of West Oakland to the nearest highway is 1 km (Apte et al., 2017).

The objective of this study is to determine which emission sources most strongly impact spatial patterns in the local air quality of Oakland. We use mobile sampling with aerosol mass spectrometry (AMS) to investigate spatial gradients in concentrations and chemical composition of OA across the three distinct areas of Oakland: port, residential West Oakland, and downtown. Additionally, using positive matrix factorization of AMS data (Ulbrich et al., 2009; Paatero and Tapper, 1994), we perform chemical source apportionment of the OA in Oakland. Results of this study not only provide valuable information on composition and source-assessment of PM_1 in Oakland, but source apportionment analysis shows how much the air quality in Oakland is impacted by local emissions versus chemically processed OA.

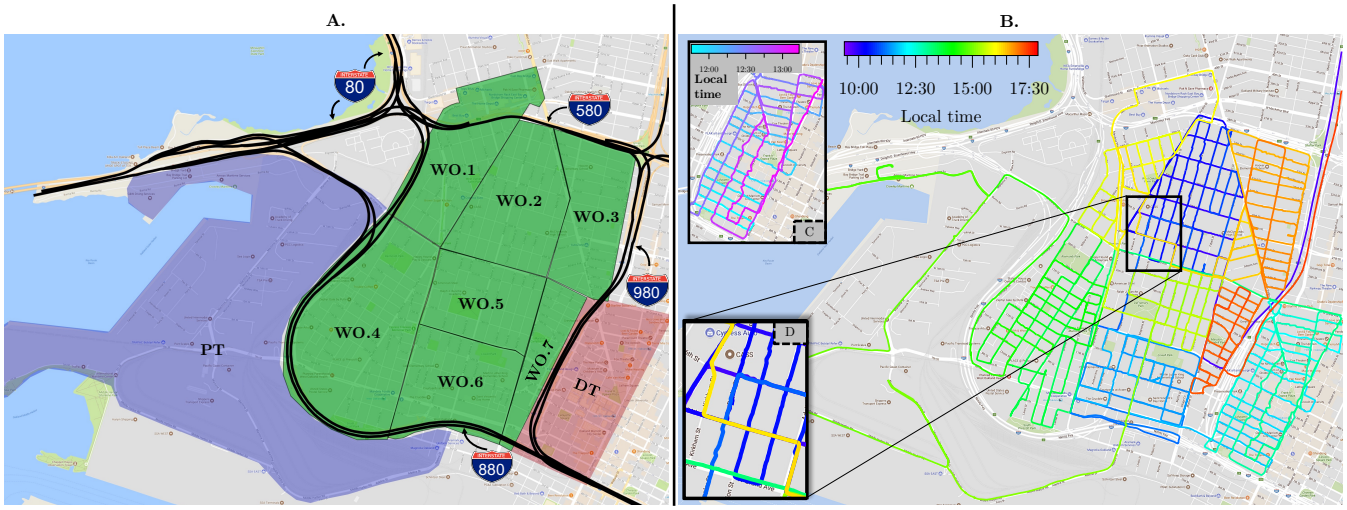

Figure 1. (a) Sampling domain with three major areas: PT (Port), WO (West Oakland) and DT (~~Downtown~~downtown). The seven internal ~~WO~~ West Oakland polygons are enumerated. (b) driving route on a typical day, showing shuffled order of polygon visits. (c) the typical driving route in downtown. (d) a zoom-in illustrating a typical repeat-sampling on the same day during inter-polygon transit

2 Experimental section

2.1 Mobile sampling

We conducted mobile sampling between 10th July and 2nd August 2017 in Oakland, CA using a mobile laboratory. Data were collected as part of the Center for Air, Climate, and Energy Solutions (CACES) air quality observatory (Zimmerman et al., 2018). The mobile laboratory is an instrumented Nissan 2500 cargo van, previously described by Li et al. (2016a, 2018). Figure 1A shows a map of the sampling domain. We sampled on all streets in the domain that were open to public traffic.

We divided the sampling domain into three main areas: Port, West Oakland and downtown. Owing to the relatively large size and road length density (16.6 km of road per km^2) of West Oakland, we further divided it into seven polygons. Port, while larger in area than West Oakland and downtown, has a very low road length density (2.6 km/km^2), because most of the area is used for parking drayage trucks and storing shipping containers. Downtown has the highest road length density (24.8 km/km^2), as would be expected in a central business district. The predominant winds in the domain are from between the north-west and south-west, as shown in Figure S17 and discussed later in Section 3.2.

Figure 1B shows the driving route on a typical day of sampling, colored by the time of day. The order in which we visited the nine polygons was shuffled daily to avoid systematically over- or under-sampling any polygon(s) in the morning, mid-day or late afternoon. Within a polygon, we employed a spiral driving pattern similar to that described by Apte et al. (2017). An exception was downtown, where, owing to alternating one-way streets, a zigzag driving pattern was used as shown in inset C in Figure 1.

2.2 Instrumentation

All instruments in the mobile laboratory were powered by a 110 V, 60 Hz alternator coupled to the van's engine. A 0.5" OD stainless steel tube carried the samples from the roof of the van ($\sim$ 3 m above ground level) to instruments as well as a mechanical backing pump. An in-line cyclone separator was installed upstream of instruments. Flow drawn by the backing pump was controlled by a needle valve such that the total flow drawn at the sampling inlet ($\sim$ 15 slpm) corresponded to a 2.5 μm cut-size diameter for the cyclone separator.

We used a high resolution time-of-flight aerosol mass spectrometer (HR-ToF-AMS, Aerodyne Research Inc.; Decarlo et al., 2006; Jayne et al., 2000) for measuring mass concentrations of non-refractory PM_1. The AMS was operated in V-mode with 20 s averaging of mass spectra. We did not collect particle time-of-flight data (used for size distribution measurements) because the additional averaging time required for collecting size distributions would decrease the overall sampling rate, compromising the goal of collecting in-motion samples with high spatial resolution. Flow was dried to $<5\%$ relative humidity prior to the AMS using a Nafion drier (MD-110-24, PermaPure). A seven-wavelength, dual-spot aethalometer (AE33, Magee Scientific) measured concentrations of black carbon with 1 min averaging per sample. We also measured CO (T300U, Teledyne API), CO_2 (LI-820, LI-COR), and particle number concentration (200P, Aerosol Dynamics Inc.) at 1 Hz sampling rate. A GPS sensor (BE-2200, Bad Elf) recorded GPS coordinates every second.

2.3 Data analysis

Timestamps and GPS co-ordinates. We first adjusted the recorded timestamps on all instrument samples based on the predetermined instrumental response times. Response times were measured by releasing a tracer at the sample inlet and recording the time lag in response from instruments while the van was stationary. This adjustment was done so as to assign each data point to the time the sample entered the inlet (as opposed to the time the data point was recorded by the instrument). Additionally, a sampling duration offset was applied to the AMS data timestamps. This is because each AMS measurement is an average of mass spectra collected for 20 s and the timestamp is assigned at the end of the 20 s period. To ensure that the sample was spatially representative of the distance traveled by the van during the 20 s sampling interval, each AMS sample was advanced 10 s in time so as to assign the measured concentration to the middle of the 20 s sampling interval, instead of the end. Next, upon alignment with GPS data, we assigned spatial coordinates to all instrument samples.

Spatial analyses. For spatial aggregation, we used a procedure similar to the "road-length snapping" procedure used by Apte et al. (2017). However, since AMS samples are recorded every 20 s and the van was driven at an average speed of 10 ms^{-1}, each AMS data point occurred roughly 200 m apart. We obtained a geospatial shapefile of Oakland's public streets from the Alameda County online archive (Alameda County, 2017). We created artificial points ("magnets") every 200 m along all streets. Multiple lanes of major surface streets were merged (i.e., opposing traffic lanes of large roads became single roadway centerlines) before creating magnets along them. This list of magnets was then matched against the GPS coordinates assigned to all AMS data points in MATLAB R2015a (MathWorks, Natick, MA) by calculating $d_{mag} = \sqrt{(y_{sample} - y_{magnet})^2 + (x_{sample} - x_{magnet})^2}$, where y are latitudes and x are longitudes. Each AMS sample was assigned

to the magnet for which it had the smallest d_{mag}. A snapping threshold of 400 m was applied to prevent samples collected outside the sampling domain (e.g., samples collected in transit to and from the overnight parking location outside the domain) from being assigned to the nearest magnet in the domain. For comparing measurements made at different sampling intervals (AMS: 20 s; BC: 1 min; CO, particle number: 1 s), we created synthetic 1 Hz AMS and BC datasets such that the measured value at the mid-point of the averaging interval was applied to all 1 second timestamps in that interval. Naturally, for 1 Hz data, the spatial resolution was not limited to 200 m, hence we used magnets spaced every 30 m (same as Apte et al., 2017).

Unique samples. The amount of time spent at a 200 m magnet can be longer than 20 s on days when driving was paused at that magnet e.g., for traffic lights, refueling stops, etc. These samples can bias a magnet's representative concentration when averaging is performed across multiple days. Conversely, as shown in the zoom-in (inset D) in Figure 1, a magnet could fall on a route used for transiting from one polygon to another on a particular day. In that case, we treat samples collected at different times of the day as independent, unique samples. This is equivalent to ascribing the same value of information to two data points collected at different times on a single day as two samples collected on different days. In order to resolve temporally clustered samples from unique samples, we averaged all samples assigned to a magnet within a 60 min window into a single unique sample. For every magnet, the median of all unique samples was chosen as a representative campaign-aggregated measurement.

Processing AMS data. We processed AMS data using SQUIRREL 1.57I and PIKA 1.16I routines in Igor Pro 6.37 (Wavemetrics, Lake Oswego, OR; Sueper et al., 2007). We applied three types of corrections to the data: (a) ionization efficiency (IE): two IE calibrations, performed before and after the campaign, provided a two-point estimate of the decay slope of IE over the 20-day period and thus a linearly increasing IE correction factor was applied to the entire AMS dataset; (b) collection efficiency (CE): a composition-dependent CE was calculated using the AMS-measured nitrate fraction in each sample (Middlebrook et al., 2012); (c) a "zero" offset, obtained daily from concentrations in particle-filtered air while the van was parked outside the sampling domain; signals recorded while sampling particle-free air were also used to resolve the very similar-mass CHO^+ ($m/z = 29.002$; particle-phase) and ^{15}NN ($m/z = 29.003$; gas-phase isotopic nitrogen) ions. Elemental ratios in this study were calculated using the "Improved-Ambient" method, which uses signal intensities of specific ion fragments to correct for biases in elemental hydrogen-to-carbon (H/C) and oxygen-to-carbon (O/C) ratios (Canagaratna et al., 2015).

Factorization of OA mass spectra. To identify sources of OA, we applied positive matrix factorization (PMF) to the two-dimensional OA matrix (time series along rows, concentrations of high-resolution organic ions up to m/z 115 along columns). PMF is essentially a bilinear deconvolution algorithm that explains the OA matrix as a linear combination of variable number of static factors and the time series of their contribution to the total OA. We performed PMF using the PMF2.exe algorithm with the ME-2 multilinear engine (Paatero and Tapper, 1994; Paatero, 2007). We explored different results within the factor-resolved solution space using the PMF evaluation toolkit (Ulbrich et al., 2009).

Accounting for temporal trends. Over the course of mobile sampling, the urban background air quality can have daily and diurnal variations due to meteorological changes (Figure S2). These variations can be accounted for with the help of concurrent stationary measurements performed at an urban background location. As discussed in Supplement Section A1, accounting for

temporal trends only had a minor ($\sim 5\%$) effect on the results. We do not include these corrections in the results presented in this manuscript.

Bootstrap resampling. In order to compare observations of OA and its factors across areas influenced by different emissions (Port, West Oakland and downtown), we first determined the precision of these measurements by resampling the ~~spatially-aggregated~~ pool of data occurring in these areas. The strength (i.e., number of ~~samples~~elements) of a bootstrapped dataset was the same as the strength of the dataset collected in that area. ~~Bootstrapping was performed with replacement and was repeated 10^4 times . We~~ For instance: $\mathbf{M} = \{m_1, m_2, ...m_n\}$ was the original set of n measurements performed in an area (e.g., Port). From all n measurements in $\mathbf{M}$, a measurement was randomly drawn to populate a synthetic set $\mathbf{M'_1}$. Each random draw was from the original set $\mathbf{M}$ with replacement i.e., independent of previous draws. The synthetic set $\mathbf{M'}$ was populated until its strength was n (same as of the original set $\mathbf{M}$). Generating such synthetic sets 10^4 times resulted in a bootstrapped pool $\mathbf{M_B}=\{\mathbf{M'_1}, \mathbf{M'_2}, ...\mathbf{M'_{10^4}}\}$. From this, a bootstrap statistic set, $\mathbf{S} = \{\tilde{s}_1, \tilde{s}_2, ...\tilde{s}_{10^4}\}$, was created where $\tilde{s}_i$ was the median of the synthetic set $\mathbf{M_i}$. Finally, the difference between 5^{th} and 95^{th} percentile of all elements of $\mathbf{S}$ was used as a dispersion statistic of the median. This results in a bootstrapped median and its 95% confidence interval for the area whose data were chosen to be the original dataset $\mathbf{M}$. We thus use the 95% confidence interval of the median as the precision of our measurements. Spatial differences larger than this precision are then deemed statistically significant. We are not aware of any prior studies that report precision of OA factors.

3 Results and discussion

In Figure ~~??~~2, we show ~~three~~ two overall results. First, we show the median aggregated OA concentrations at each magnet. OA is spatially variable, with the highest concentrations typically observed downtown ~~. Second, the spatial coverage of the AMS dataset is expressed using marker sizes as a function of number of unique samples collected at each magnet. Further, inset A shows cumulative distributions of raw and unique samples across the entire range of magnets. Approximately 60% of the magnets are represented by more than 10 unique samples, suggesting that our data are indicative of long-term spatial patterns (Apte et al., 2017).~~

~~Lastly, inset B in Figure ??~~ and along I-880, the highway used by drayage trucks to approach the Port. Second, the pie chart in Figure 2 shows the campaign-median contributions of organics (Org), sulfate (SO_4^{2-}), nitrate (NO_3^-), ammonium (NH_4^+), chloride (Cl^-) and black carbon (BC) to the total PM_1. The clear dominance of organics along with relative contributions of other species are similar to previously published AMS measurements performed in other urban areas (Hayes et al., 2013; Ortega et al., 2016; Mohr et al., 2015). Further, Figure S4 shows cumulative distributions of raw and unique samples across the entire range of magnets. Approximately 60% of the magnets are represented by more than 10 unique samples, suggesting that our data are indicative of long-term spatial patterns (Apte et al., 2017).

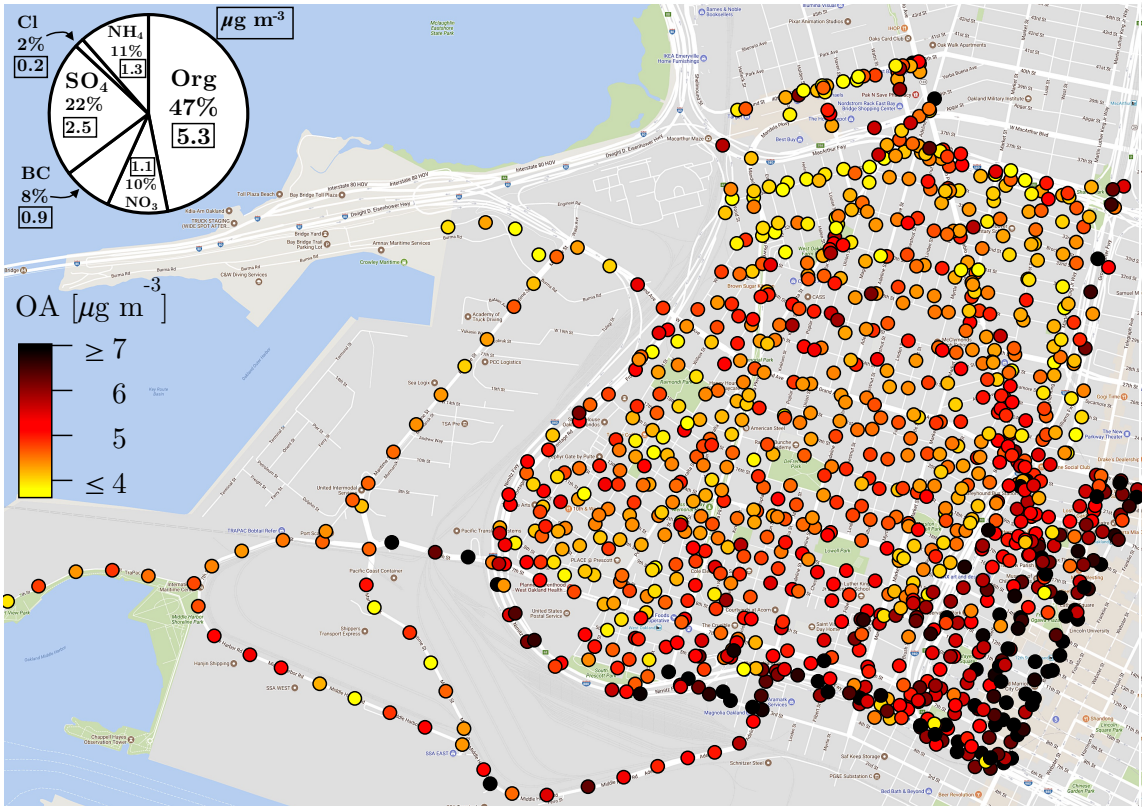

Figure 2. Median organic aerosol concentration at each magnet~~and sampling coverage map of the domain~~. ~~Inset (a): Cumulative distribution of raw and unique samples in all magnets in domain. Inset (b):~~ The pie chart shows median contribution of AMS-measured non-refractory [organics (Org), sulfate (SO_4^{2-}), nitrate (NO_3^-), ammonium (NH_4^+), chloride (Cl^-)] and aethalometer-measured black carbon (BC) to the total PM_1. ~~Underlined~~ Boxed values are absolute mass concentrations in μ~~gm~~g m^{-3}.

3.1 Organic aerosol (OA)

We now discuss the spatial patterns of OA in more detail. Figure 3 compares the OA concentrations across the three areas (Port, West Oakland and downtown) using cumulative distribution function (CDF) curves in the upper panel. OA concentrations are spatially variable within each sampled area. A range of ~~$> 2\mu$gm~~$> 2\ \mu$g m^{-3} is observed in the median OA concentrations at all magnets of each area.

The lower panel of Figure 3 shows the central tendency statistics (mean, median and standard deviation) of the values assigned to magnets in each area. The data are positively skewed in all polygons i.e., the mean is higher than the median. Ambient measurements typically exhibit a positively-skewed distribution under the influence of local emission events ~~(Apte et al., 2017; Van den Bossche et al., 2015; Brantley et al., 2014)~~(Seinfeld and Pandis, 2006; Apte et al., 2017; Van den Bossche et al
Hence, the median is chosen over the mean as a central tendency statistic to discuss the OA spatial patterns. The results shown

in this figure are reinforced with statistical confidence by using bootstrap resampling (Figure S5). We determined a precision of 0.5 μgmg m^{-3} in the median OA. Spatial differences larger than this precision are considered statistically significant.

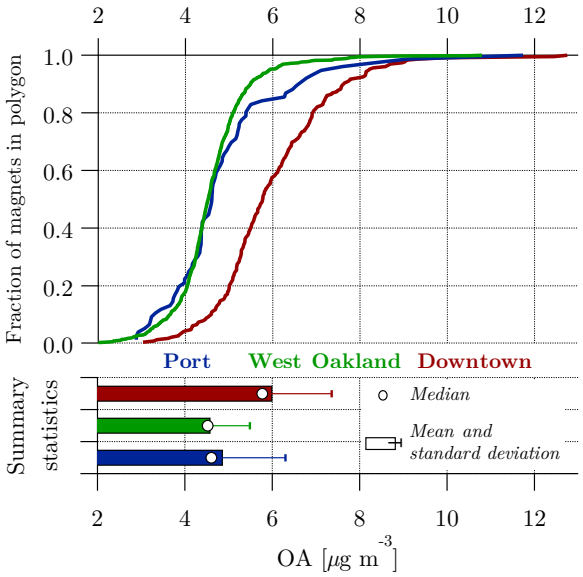

Figure 3. Cumulative distributions, mean and median of OA concentrations in Port, West Oakland and downtown.

Downtown has a median OA concentration of 5.7 μgmg m^{-3}, which is 27% higher than West Oakland and Port. Almost the entire downtown CDF curve is $\sim$ 1.5 μgmg m^{-3} greater than the West Oakland and Port curves, indicating that all parts of downtown have higher OA concentrations than the rest of Oakland. Port and West Oakland have similar OA concentrations, as evidenced by their nearly-superimposed CDFs and similar medians (4.6 ± 0.05 μgmg m^{-3}). However, Port measurements have more positive skewness than West Oakland; Port has a larger fraction of magnets with high OA concentrations than West Oakland. This suggests that the OA concentrations in Port are more influenced by local emission events. As mentioned earlier, Port has a high drayage truck activity, which likely explains this skewness. Results from bootstrapping support this explanation (Figure S5). Port data have a higher mean (4.9 μgmg m^{-3}) with a wider 95% confidence interval (0.7 μgmg m^{-3}) about this mean, compared to West Oakland (mean: 4.6 μgmg m^{-3}; 95% confidence interval about the mean: 0.2 μgmg m^{-3}).

3.2 ~~Black carbon (BC)~~

~~In this subsection, we investigate the influence of higher drayage truck activity on air quality in Port of Oakland. In addition to OA, BC is a prominent component of particulate emissions from heavy-duty diesel trucks (Ban-Weiss et al., 2008; ?).The use of diesel particulate filters and catalytic reducers has substantially reduced BC emissions from drayage trucks in Oakland (Dallmann et al., 2011; Preble et al., 2015). However, ? reported that diesel trucks contribute 45% of BC concentrations in the Caldecott tunnel in Oakland, despite being a minor ($<$ 1%) fraction of their sampled vehicle fleet. It is thus reasonable to expect~~

that while the vast majority (99%) of the truck fleet at the Port of Oakland is now equipped with advanced emission control technologies, the overall large volume of trucks arriving in the area results in higher BC emissions than light-duty gasoline vehicles.

We use the OA/BC ratio to distinguish car and truck emissions, with the underlying assumption that these use gasoline and diesel combustion, respectively. By extension, areas with smaller ambient OA/BC would indicate a larger influence from diesel truck emissions. Because OA and BC measurements were made at different sampling frequencies, we compare these measurements by first converting them to a synthetic 1 Hz timeframe as described earlier. A map of median OA/BC values at each 30 m magnet is shown in Figure **??**.

Fine-scale map of median OA/BC values (unitless).

In general, areas with lower OA/BC values are streets and highways approaching the Port of Oakland (e.g., Interstate 880 and the surface street connecting it to the port) as well as those around centers of shipping commerce in the Port. This is expected because trucks are found idling while in queue outside these facilities. Bootstrap resampling the BC dataset shows that the measurements (especially in Port) have a considerable positive skew. The ratio of mean to median BC in Port is higher (1.5) than both West Oakland and downtown (1.2). Because BC concentrations are largely influenced by local sources (diesel trucks), the large amount of drayage trucks in Port likely causes the mean BC to be $\sim$ 8% higher than downtown, even though median BC in downtown is $\sim$ 7% higher than Port. This finding suggests that despite substantial reductions in BC emissions from diesel trucks by the use of particulate filters and catalytic reducers, the influence of diesel truck emission plumes on the air quality in Port is higher than that in downtown.

3.2 OA factors

We identified three OA factors with distinct mass spectra using positive matrix factorization (PMF) of AMS data: hydrocarbon-like OA (HOA), cooking OA (COA) and semi-volatile less-oxidized oxygenated OA (SV-OOALO-OOA). These factor profiles are shown in Figure 4. Distinct features of each factor mass spectra (e.g., signals at particular m/z's and elemental O/C ratios) as well as the diurnal patterns in their time series are used to characterize these factors. We use the same nomenclature for these factors as has been used commonly in literature. For comparison, previously reported mass spectra of these factors are shown in Figure S9.

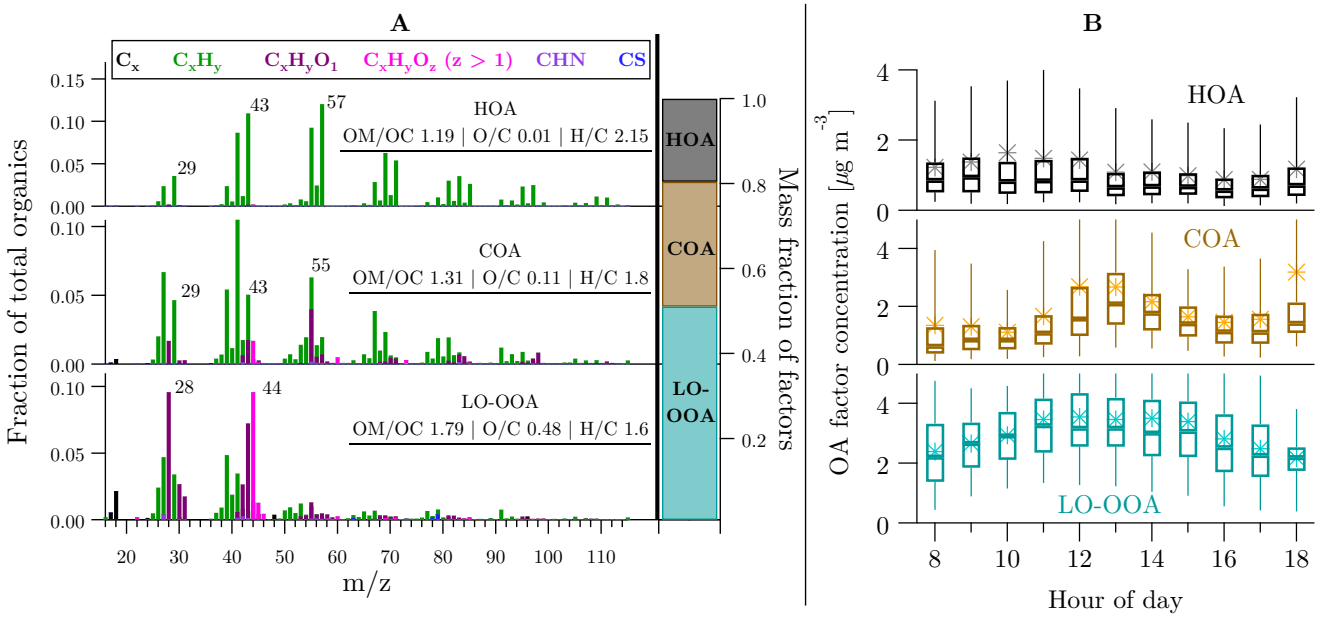

Figure 4. (a) Mass spectra, elemental ratios and average mass fraction of factors obtained from PMF analysis of all AMS spectra. (b) Boxplot of diurnal profiles of factors: rectangles enclose 1st through 3rd quartiles of data. Horizontal bars are medians. Asterisk markers are means. Whiskers are 5th and 95th percentiles.

HOA: The HOA factor has an elevated signal at the series of C_nH_{2n+1} (e.g., $C_4H_9^+$ at m/z 57) and C_nH_{2n-1} (e.g., $C_3H_5^+$ at m/z 41). Previous studies have identified this factor as a marker of fresh vehicular emissions based on its reduced state (O/C = 0.01) as well as its diurnal pattern (elevated during morning and evening traffic rush periods; Zhang et al., 2011; Mohr et al., 2012). HOA time series are highly positively skewed (average of hourly mean/median = 1.6) even during non-peak periods, which indicates influence of local HOA plumes.

COA: The COA factor has a distinct signal at m/z 55 ($C_4H_7^+$ and $C_3H_3O^+$). Previous studies have identified this factor as a marker of cooking emissions based on its reduced state (O/C = 0.11) as well as its diurnal pattern (elevated concentrations occurring typically during lunch and dinner time; Mohr et al., 2009, 2012; Zhang et al., 2011). Similar to HOA, COA time series are also highly positively skewed (average of hourly mean/median = 1.53), indicating influence of local COA plumes.

~~SV-OOA~~LO-OOA: Compared to the HOA and COA factors, this factor is relatively more oxygenated with a distinct peak at m/z 44 in its mass spectrum. Secondary OA contains oxygen-containing groups (e.g., carboxylic acids, alcohols and carbonyls). These groups, upon ionization in the AMS, contribute to the m/z 44 (COO^+) signal. Generally, based on increasing extent of atmospheric processing~~(and, by extension, decreasing volatility),~~ , two classes of oxygenated OA are identified by signals at m/z 43 and 44: ~~SV-OOA and low-volatility oxygenated OA (LV-OOA) (Donahue et al., 2012; ?)~~less- and more-oxidized oxygenated OA (LO-OOA and MO-OOA, respectively; Xu et al., 2015). Of these two, ~~SV-OOA~~ LO-OOA is relatively less oxygenated, bears similarity to semi-volatile OOA (SV-OOA) in the two-dimensional volatility basis set

(Donahue et al., 2012), and is considered "fresh SOA" formed by gas-phase oxidation of organic precursors emitted nearby (Hayes et al., 2013). ~~SV-OOA~~ LO-OOA is thus found to be strongly correlated with particulate NO_3^-.

Having made no thermodenuded measurements of OA volatility, we identify the third, oxygenated factor in our PMF solution as ~~SV-OOA~~ LO-OOA because (a) the mass spectrum and elemental ratios are similar to those reported for LO-OOA (and SV-OOA) elsewhere (Figure S9), and (b) this factor is correlated with AMS-measured NO_3^- signal (Figure S10). The diurnal pattern of the ~~SV-OOA~~ LO-OOA factor has a more normal distribution about mid-day. Additionally, the ~~SV-OOA~~ LO-OOA time series exhibit less positive skewness (average of hourly mean/median = 1.07) compared to COA and HOA. Compared to the two primary factors, ~~SV-OOA~~ LO-OOA in Oakland has less spatial variability.

Contribution of OA factors: Average contributions of COA, HOA and ~~SV-OOA~~ LO-OOA to total OA are shown in Figure 4. COA and HOA collectively contribute $\sim 45\%$ of the total OA mass. This fraction of primary contributions to OA is higher than that reported for typical urban OA in prior studies ~~(Zhang et al., 2007)~~(Zhang et al., 2007; Crippa et al., 2013b). Through mobile measurements in Pittsburgh, PA, Gu et al. (2018) find that $\sim$ 25-30% of the annual average OA mass is primary. The relatively high contributions of primary OA suggest that OA in Oakland is more strongly influenced by local emissions than other locations.

Previous AMS-PMF studies have reported the presence of both ~~SV- and LV-OOA~~ LO- and MO-OOA factors in ambient OA. The absence of an ~~LV-OOA~~ MO-OOA factor in Oakland can be explained by the hypothesis that air masses arriving in Oakland are oceanic. These air masses are expected to contain very low OA concentrations, even though most of this OA is highly oxidized ~~LV-OOA~~ MO-OOA (Hildebrandt et al., 2010). The ~~LV-OOA~~ MO-OOA in these oceanic air parcels would be rapidly overwhelmed by urban emissions as the air parcels are advected over San Francisco and Oakland, resulting in apparent absence of an ~~LV-OOA~~ MO-OOA factor in Oakland. This hypothesis of predominantly oceanic air masses is confirmed by the wind rose diagrams in Figure S17. Predominant winds measured at the Oakland anemometer during periods of mobile sampling are from between the north-west and south-west with typical wind speeds of $\sim$ 10 kmh^{-1}. This means that Oakland falls roughly 60 min downwind from the Pacific Ocean. Emissions from the metropolitan SF area are likely advected to Oakland, although the timescale of this advection is <60 min. On this timescale, ~~SV-OOA~~ LO-OOA formation from the SF emissions could be expected, but ~~LV-OOA~~ MO-OOA formation in amounts such that it would be detectable after mixing with the local emissions in Oakland is not expected (Decarlo et al., 2010; Jimenez et al., 2009). The ~~SV-OOA~~ LO-OOA factor profile shown in Figure 4 has a minor contribution from methanesulfonic acid (m/z 79), which was previously found to be an indicator of marine origin of air parcels ~~(?)~~(Crippa et al., 2013a). This finding confirms that the air masses arriving in Oakland are predominantly oceanic.

Quality of PMF solution: PMF decomposes measured OA concentrations using a linear combination of contributions from static factors. The amount of observed mass that cannot be explained by the reconstructed factor contributions is binned into residual mass. Residuals of factorization are shown in Figure S11. The ratio of scaled residuals, Q, to the total degrees of freedom of the fitted data, Q_{exp} would be ≈ 1 in a perfect factorization (Ulbrich et al., 2009). PMF numerically approaches a convergence using different initial starting points (f_{peak}) in the rotational domain about zero (Paatero and Tapper, 1994). Values of Q/Q_{exp} for different values of f_{peak} are shown in Figure S14, along with the factor mass fractions for each solution.

Our 3-factor PMF solution is very stable ($1.42 < Q/Q_{exp} < 1.43$) and the factor mass fractions do not change with varying f_{peak}.

A 4-factor solution was also examined (Figure S12). While the mass spectra and fractional contributions of both HOA and COA remain unchanged from the 3-factor solution, the ~~SV-OOA~~ LO-OOA factor from the 3-factor solution was further deconvolved into a more oxygenated ~~LV-OOA~~ MO-OOA factor and a fourth less oxygenated factor that bore no similarity to the typical ~~SV-OOA~~ LO-OOA factor spectra reported in the literature. We discarded this 4-factor solution because (a) given that fresh OA factors (HOA and COA) as well as OOA factors form a continuum of atmospheric oxygenation, we do not expect the presence of the fresh OA and ~~LV-OOA~~ MO-OOA factors while an ~~SV-OOA~~ LO-OOA factor is absent, (b) we did not find a strong PMF-independent tracer correlation (e.g., with AMS-measured particulate NO_3^- or SO_4^{2-}) for the ~~LV-OOA~~ MO-OOA and the fourth factor, and (c) going from 3-factor to 4-factor solution, there was only a 5% reduction in Q/Q_{exp}, suggesting not only diminishing returns with number of factors ~~>~~ 3~~>~~ 3, but simply an artificial splitting of the optimal solution, which would result in an overinterpretation of the PMF results (Ulbrich et al., 2009). This artificial splitting is also evidenced and discussed later using elemental analysis in Section 3.5.

3.3 Spatial and temporal variability of OA ~~and its~~ factors

In this section, we further analyze the spatial and temporal patterns of OA and its factors. We begin with examining the primary-secondary split of OA and how this split varies across space and time. Understanding variability in the primary fraction of OA is important because we know from recent findings that in close proximity to sources such as highways (Saha et al., 2018b), and restaurants (Robinson et al., 2018), there is high amount of primary OA mass in Aitken-mode particles ($<$ 100 nm diameter; Ye et al., 2018) and the particle population is externally-mixed. Atmospheric processing of these emissions (e.g., increasing SOA fraction, coagulation with background particles) makes the particle size distributions more unimodal and internally-mixed in the accumulation mode (200-1000 nm diameter range; Ye et al., 2018). This primary-secondary split may have important health exposure implications because Aitken-mode particles have longer retention times once they penetrate lung tissue ~~(Ferin et al., 1992; ?; Stölzel et al., 2007)~~(Ferin et al., 1992; Oberdörster, 2000; Stölzel et al., 2007).

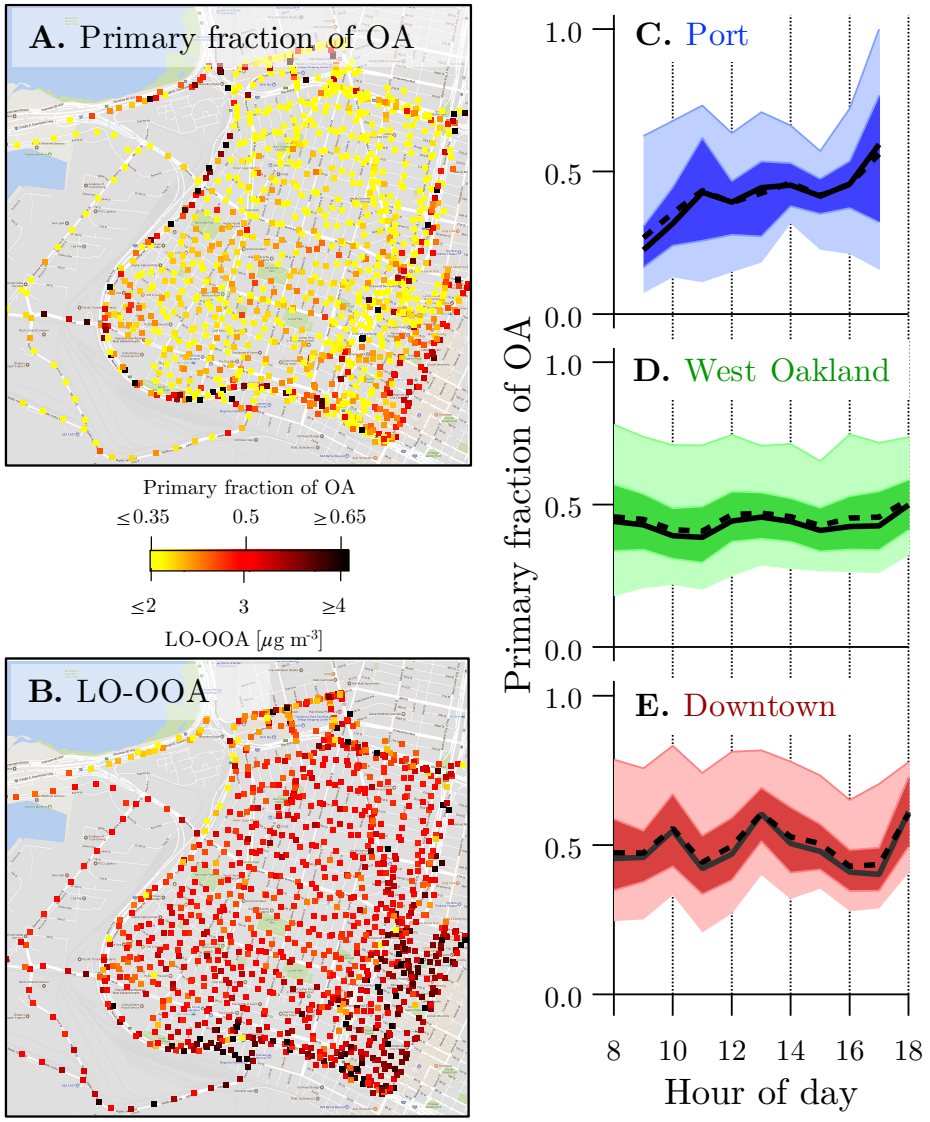

Figure 5. (a) Median primary fraction of OA at each magnet. Primary fraction is defined as the ratio of COA + HOA to the total OA at each magnet. (b) Median LO-OOA concentration at each magnet. Also shown are diurnal profiles of the primary OA fraction in (c) Port, (d) West Oakland, and (e) downtown. Solid and dashed lines are hourly medians and means, respectively. Darkly-shaded areas enclose 1st and 3rd quartiles of data. Lightly-shaded areas enclose 5th through 95th percentiles of data.

Overall, the OA mass in Oakland is split into primary and secondary factors roughly evenly (Figure 4): two primary factors (COA + HOA) collectively contribute ∼ 45%, while the rest is secondary (~~SV-OOA~~LO-OOA). However, the primary/secondary split at each magnet is spatially and temporally variable. To identify areas with elevated levels of primary emissions, we normalized the sum of COA and HOA to the total OA concentration at each magnet, which results in a primary fraction of the OA at the magnet. In Figure 5A, we show a map of primary fraction of OA at each magnet in the domain. It is evident that the

OA in parts of downtown has a higher than 50% contribution from primary sources. Other areas exhibiting higher fractions of primary sources are the highways. In the more residential areas (West Oakland), ~~SV-OOA~~ LO-OOA contributes ~ 55% of the OA (Figure 5D). Through bootstrap resampling, a precision of ~ 1.5% was determined for the primary fraction of OA (Figure S6).

Figure 5B shows a map of the ~~SV-OOA~~ LO-OOA mass concentrations. While ~~SV-OOA~~ LO-OOA has a smoother spatial pattern than primary OA, downtown exhibits higher ~~SV-OOA~~ LO-OOA concentrations. Individual maps of COA and HOA are shown in Figure S18. Figure 5 also shows the diurnal profiles of the primary contributions to OA in Port, West Oakland and downtown. The primary OA contributions in Port and downtown are more temporally variable than in West Oakland. Generally, primary OA contributions in Port have a positive trend (from ~ 25% to 60%) with increasing hour of day, with peaks occurring at ~ 11 AM and 6 PM. This is likely due to increasing volume of trucks as the day progresses. By contrast, primary contributions in downtown are consistently around 50% of the total OA, with peaks during high traffic periods and lunch time. Primary contributions in West Oakland are consistently around 45%, with no distinct peaks.

~~(a) Median primary fraction of OA at each magnet. Primary fraction is defined as the ratio of COA + HOA to the total OA at each magnet. (b) Median SV-OOA concentration at each magnet. Also shown are diurnal profiles of the primary OA fraction in (c) Port, (d) West Oakland, and (e) downtown. Solid and dashed lines are hourly medians and means, respectively. Darkly-shaded areas enclose 1st and 3rd quartiles of data. Lightly-shaded areas enclose 5th through 95th percentiles of data.~~

Figure 6 shows a scatter plot of COA versus HOA contributions to OA from the entire campaign, which is meant to show the diurnal variation of primary OA sources. During the morning rush hour, concentrations of COA and HOA are roughly equal. Primary OA concentrations start transitioning towards COA dominance at ~ 11 AM, which co-incides with the typical time restaurant kitchens would be expected to begin activity. By ~ 2 PM, COA dominates the primary OA mass.

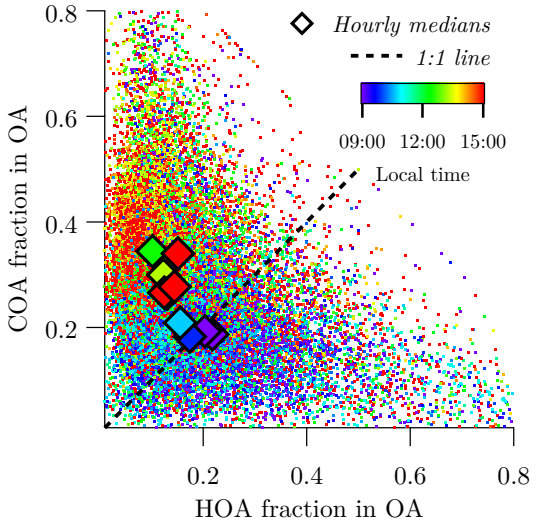

Figure 6. Diurnal shift of source of primary OA from morning rush hour traffic to mid-day cooking activities. Dots show individual measurements and diamonds show hourly medians over the entire sampling campaign.

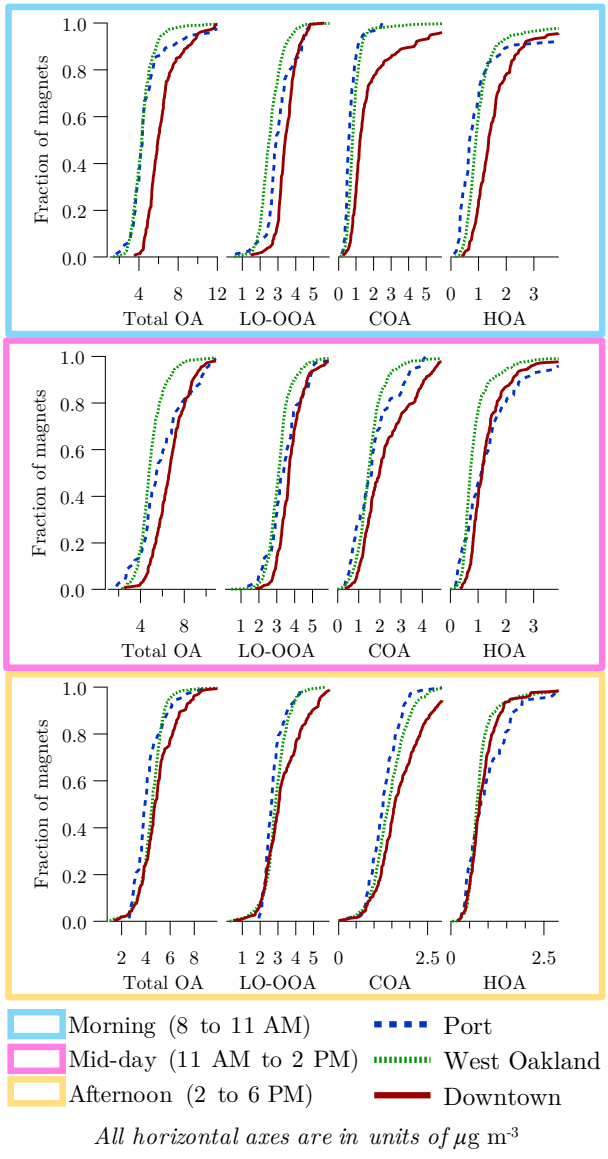

Figure 7. Cumulative distribution functions of total OA as well as the three factors identified in this study, resolved by area (Port, West Oakland and downtown) and time of day: morning (8 to 11 AM), mid-day (11 AM to 2 PM) and afternoon (2 to 6 PM). The colored box around each set of CDFs indicates the period of the day those data represent.

In Figure 7, we show the spatial and temporal patterns of total OA as well as the three OA factors by resolving them by area (Port, West Oakland and downtown) and time of day: morning (8 to 11 AM), mid-day (11 AM to 2 PM) and afternoon (2 to 6 PM). To aid discussion with statistical confidence, we refer the reader to Figure S7, which shows 95% confidence intervals of these results obtained from bootstrap resampling. As described earlier, we consider the 95% confidence interval of the

bootstrapped median as an indicator of precision i.e., spatial differences larger than this precision are deemed statistically significant. Overall, OA factors have a ~ 0.25 μgmg m^{-3} precision. This precision agrees with that determined in an independent dataset acquired in Pittsburgh, PA (Gu et al. *in prep.*). (Gu et al., 2018).

Cumulative distribution functions of total OA as well as the three factors identified in this study, resolved by area (Port, West Oakland and Downtown) and time of day: morning (8 to 11 AM), mid-day (11 AM to 2 PM) and afternoon (2 to 6 PM). The colored box around each set of CDFs indicates the period of the day those data represent.

OA. During the morning period (8 to 11 AM), the median OA concentration in downtown is 40% (~ 1.7 μgmg m^{-3}) higher than in West Oakland and Port. Median OA in Port and West Oakland are similar (within precision). On average, the median OA concentration in the entire domain is 16% (~ 0.8 μgmg m^{-3}) higher during mid-day (11 AM to 2 PM), compared to the morning period. Median OA concentration in downtown is 40% (~ 1.9 μgmg m^{-3}) higher than in West Oakland and 21% higher than in Port. During the afternoon (2 to 6 PM), the median OA concentration over the entire domain is 20% (~ 1.2 μgmg m^{-3}) lower than the mid-day period. Median OA concentration in downtown is similar to West Oakland (4.6 ± 0.14 μgmg m^{-3}) and 17% higher than in Port. Overall, total OA concentrations in downtown are consistently higher than Port and West Oakland during morning, mid-day and afternoon periods.

HOA. During the morning period, median HOA concentration in downtown is 52% (~ 0.5 μgmg m^{-3}) higher than in West Oakland. Median HOA concentration in West Oakland, in turn, is 32% higher than Port. There is no net increase in median HOA concentration in the entire sampling domain from morning to mid-day. However, from morning to mid-day, the median HOA reduces by 16% and 20% in downtown and West Oakland respectively, while that in Port increases by 64% (~ 0.4 μgmg m^{-3}). As a result, during mid-day, the median HOA in downtown and in Port are similar (1.1 ± 0.01 μgmg m^{-3}), and higher than that of West Oakland by 58% (~ 0.4 μgmg m^{-3}). On average, the median HOA concentration in the entire domain is ~ 0.2 μgmg m^{-3} lower during the afternoon compared to the mid-day and morning periods. Median HOA concentrations in the three polygons are all similar 0.8 ± 0.06 μgmg m^{-3}, with Port being highest.

Overall, HOA is highest in downtown in the morning, despite the fact that all of Oakland has roughly equal proximity to highways. While we do not have detailed traffic data for Oakland, it is reasonable to assume that downtown receives a large influx of commuters during the morning rush hour and thus would be expected to have the highest HOA concentrations. Downtown also has a higher road length density compared to West Oakland and Port, and as a result, can accommodate a larger traffic volume per km^2. Further, poor ventilation of vehicle emissions in downtown can also contribute to higher HOA levels (Yuan et al., 2014). During mid-day and afternoon, however, Port has similar or higher HOA than downtown. This is expected for two reasons: (a) the commuters contributing to high HOA in downtown during the morning hours are working (and their cars parked) during midday, and (b) the high amount of drayage truck activity in Port. There is some evidence from fuel sales data that truck activity at the Port is higher in the afternoon than the morning. One of the measures implemented to reduce Port emissions was to keep shipping logistics gates open in the evening to dilute daytime congestion of drayage trucks (Port of Oakland, 2016), which may contribute to trucks at the Port not following the typical rush hour traffic patterns of commuters. West Oakland has the lowest HOA concentrations at all times of day, as would be expected for a largely residential area.

COA. Median COA concentration in downtown is 55% ($\sim$ 0.5 μ~~gm~~g m^{-3}) higher than in West Oakland and 109% higher than in Port during the morning period. Further, COA concentrations in downtown exhibit a larger positive skew (mean/median = 1.5) relative to both West Oakland and Port (mean/median = 1.15). On average, the median COA concentration in the entire domain is $\sim$ 0.8 μ~~gm~~g m^{-3} higher during mid-day, compared to the morning period. Median COA concentration in downtown is 27% higher than in West Oakland and Port during mid-day. On average, the median COA concentration in the entire domain is $\sim$ 0.3 μ~~gm~~g m^{-3} lower during the afternoon compared to the mid-day period. Median COA concentration in downtown is 11% and 26% higher than in West Oakland and Port, respectively.

Overall, COA is consistently highest in downtown, which is not surprising given the large number of restaurants in downtown. The spatial distribution of COA in West Oakland and Port is uniformly low in the morning, as demonstrated by the steepness of the distribution functions in Figure 7. During mid-day and late afternoon, however, COA levels in both these areas are higher than in the morning. It is not clear why COA in Port is higher than ~~WO~~ West Oakland during mid-day. It should be noted, however, that due to the considerably low road length density in Port, the number of magnets in Port is only $\sim$ 10% of those in West Oakland. As a result, even a few cooking sources in Port (most likely food trucks) could cause the spatially aggregated values for Port appearing to be higher than West Oakland. Overall, Port has the lowest COA concentrations, which is expected given the land use in that area.

~~*SV-OOA*~~*LO-OOA*. Median ~~SV-OOA~~ LO-OOA concentration in downtown is 36% ($\sim$ 0.9 μ~~gm~~g m^{-3}) and 17% higher than in West Oakland and Port, respectively, during the morning period. On average, the median ~~SV-OOA~~ LO-OOA concentration in the entire domain is 15% ($\sim$ 0.5 μ~~gm~~g m^{-3}) higher during mid-day than the morning period. ~~Median SV-OOA~~ During mid-day, median LO-OOA concentration in downtown is 18% ($\sim$ 0.6 μ~~gm~~g m^{-3}) higher than in West Oakland and 8% higher than in Port. On average, the median ~~SV-OOA~~ LO-OOA concentration in the entire domain is 20% ($\sim$ 0.5 μ~~gm~~g m^{-3}) lower in the afternoon, compared to the mid-day period. Median ~~SV-OOA~~ LO-OOA concentrations in all three areas are similar (2.9 ± 0.2 μ~~gm~~g m^{-3}), with downtown being the highest and Port being lowest.

~~SV-OOA~~ LO-OOA concentrations are consistently higher in downtown compared to Port and West Oakland. This finding is unexpected because ~~SV-OOA~~ LO-OOA is secondary; the null hypothesis for secondary species is that concentrations would be spatially uniform. Multiple lines of evidence contribute to the conclusion that ~~SV-OOA~~ LO-OOA is indeed higher in downtown than the Port and West Oakland. First, as shown in Figures 7 and S7, morning-time ~~SV-OOA~~ LO-OOA concentrations are 0.9 and 0.5 μ~~gm~~g m^{-3} higher in downtown than in Port and West Oakland. Given our determined precision of 0.25 μ~~gm~~g m^{-3} in OA factors, these spatial differences are significant. As ~~discussed above and~~ shown in Figure S1, our sampling times are not temporally biased; therefore, higher ~~SV-OOA~~ LO-OOA downtown does not appear to be an artifact of our sampling strategy (e.g., downtown is not oversampled at midday relative to West Oakland and Port). Second, the ~~SV-OOA~~ LO-OOA CDFs in Figure 7 are further substantiated by East-West transect drives performed during inter-polygon transits on different days of the campaign and shown in Figure 8. These transects show that there is a general trend of increasing ~~SV-OOA~~ LO-OOA concentrations between the Port and downtown. Third, the enhanced ~~SV-OOA~~ LO-OOA downtown echoes similar measurements made independently in Pittsburgh, where fresh SOA is also enhanced in the downtown area ~~(Gu et al. *in prep.*).~~ (Gu et al., 2018).

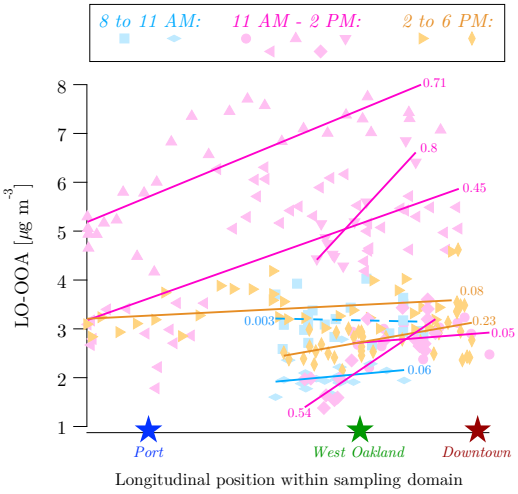

Figure 8. Spatial variations in measured ~~SV-OOA~~ LO-OOA on select intra-polygon transit drives on different days, colored by three different diurnal time periods. Drives that reasonably spanned the longitudinal extent of the sampling domain with minimal latitudinal displacement were picked for this plot. Markers are individual ~~SV-OOA~~ LO-OOA samples and lines are fits for each transect drive. Fits that have a positive slope with proximity to downtown are shown as solid lines. The only fit that has a negative slope is shown as a dashed line. R^2 of fits are shown next to fits. Approximate locations of Port, West Oakland and downtown are shown as references to better visualize longitudinal positions of data.

~~Higher concentrations of SV-OOA in downtown suggest that there is enhanced photochemical activity in that area.~~ The increasing concentrations of LO-OOA with increasing inland distance (Figure 8) can be explained by the predominant Westerly winds (Figure S17). At the typical wind speed of $\sim$ 15 kmph, downtown is 10-15 min downwind from the Port. The additional processing of OA in this time can result in higher LO-OOA in downtown. However, we also observe that the spatial pattern of LO-OOA changes diurnally, with a stronger spatial gradient in the morning than the afternoon (Figure 7). This suggests that the local photochemical microenvironment may also contribute to the observed LO-OOA spatial pattern.

Enhanced photochemical production of SOA could be due to several reasons. Firstly, the pool of reactive SOA precursor vapors is likely enhanced in downtown relative to other areas. We show above in Figure 7 that HOA is highest in downtown. HOA is co-emitted with volatile and intermediate-volatility organic compounds that efficiently generate SOA upon photochemical oxidation (Robinson et al., 2007; Gordon et al., 2013; Zhao et al., 2015).

Secondly, concentrations of the hydroxyl (OH) radical may also be higher downtown. The OH radical is the dominant daytime oxidizing agent, especially for reduced compounds emitted from motor vehicles. It has been shown that in urban, polluted environments (street canyons), high-NO_x emissions from vehicles render increased levels of nitrous acid (HONO), which in turn results in increased local oxidation capacity (Yun et al., 2017; Villena et al., 2011) due to rapid photolysis of HONO to OH (Stutz et al., 2000; Finlayson-Pitts and Pitts, 2000; Zhong et al., 2017).

A third factor may also contribute to higher precursor concentrations, and therefore additional ~~SV-OOA~~LO-OOA, in downtown. The presence of tall buildings in downtown can create higher surface roughness, which in turn can reduce pollutant dispersion and promote internal recirculation (Zhong et al., 2017). This possibility is further examined in Figure S19, which shows building heights in downtown. Downtown has relatively taller buildings that collectively act as a wall parallel to the Interstate 980 highway upwind. The air masses in downtown may experience stagnation and poor ventilation relative to West Oakland and Port. This, in turn, can increase the reaction time, thereby allowing more local ~~SV-OOA~~ LO-OOA formation.

The combined impact of vehicle emissions on OH (via HONO) and gas-phase precursor concentrations in downtown would be expected to be largest in the morning, since these are co-emitted with HOA. Indeed, the largest enhancement of ~~SV-OOA~~ LO-OOA in downtown occurs in the morning hours, at the same time as the largest enhancement of HOA. From morning to mid-day, ~~SV-OOA~~ LO-OOA concentrations become more spatially uniform; median ~~SV-OOA~~ LO-OOA concentrations in West Oakland and Port increase by 23% (0.6 μ~~gm~~g m^{-3}) and 16% (0.5 μ~~gm~~g m^{-3}) respectively, while downtown only increases by 7% (0.25 μ~~gm~~g m^{-3}). This suggests that while downtown has high photochemical activity in the morning, the entire sampling domain transitions towards a more uniform photochemical state by mid-day.

We further investigated the enhanced photochemical activity in downtown by analyzing mobile measurements of particulate sulfate (SO_4^{2-}). SO_4^{2-} is formed upon reaction of gas-phase SO_2 with OH (Miyakawa et al., 2007), which can be enhanced in polluted environments due to catalytic involvement of black carbon particles (Novakov et al., 1974). Figure S8 shows that SO_4^{2-} concentrations in downtown are higher ($\sim$ 8%) than Port and West Oakland, a trend similar to that observed in ~~SV-OOA~~ LO-OOA concentrations.

Ships associated with the Port are the major source of SO_2 in Oakland (Tao et al., 2013). While ship SO_2 emissions have significantly decreased in recent years, ships remain the dominant SO_2 source in our sampling domain, and there seem to be no local sources of SO_2 or particulate SO_4^{2-} in downtown. Thus, elevated concentrations of secondary sulfate in downtown would therefore support the hypothesis that OH concentrations are also higher in downtown, giving rise to local variations in SO_4^{2-} formation rate.

3.4 Spatial patterns of gasoline and diesel vehicle emissions

In this subsection, we compare the influence of emissions from diesel trucks against that from gasoline-powered vehicles. We do this by comparing concentrations and ratios of OA, HOA, BC, and CO. Traditionally, diesel vehicles have significantly higher emissions of HOA and BC than gasoline vehicles (Ban-Weiss et al., 2008), whereas gasoline vehicles have higher CO emissions than diesel vehicles (May et al., 2014). Vehicle emission standards are regularly tightened, so emissions are lower for newer vehicles. However, emission reductions are not equal for all species, so the ratios of different emitted pollutants vary with both vehicle age and fuel type. Thus, the specific emissions and emission ratios from the vehicle fleet in a city, or a portion of the city, depend on both the gasoline-diesel split and the age distribution of gasoline and diesel vehicles.

Based on typical emissions from gasoline and diesel vehicles, we would expect that: (a) all areas with heavy traffic should have elevated concentrations OA, HOA, BC, and CO, and (b) diesel-dominated areas will have higher BC/CO, higher HOA/CO, and lower OA/BC ratios than gasoline-dominated or background locations. The specific concentration ratios in different areas

will be a function of the vehicle fleet in that area and the contribution of fresh emissions versus background. One potential drawback of using concentration ratios to identify gasoline- versus diesel-dominated areas is that emission ratios from cars are becoming more "diesel-like" (May et al., 2014; Saliba et al., 2017), which complicates the analysis for newer vehicle fleets.

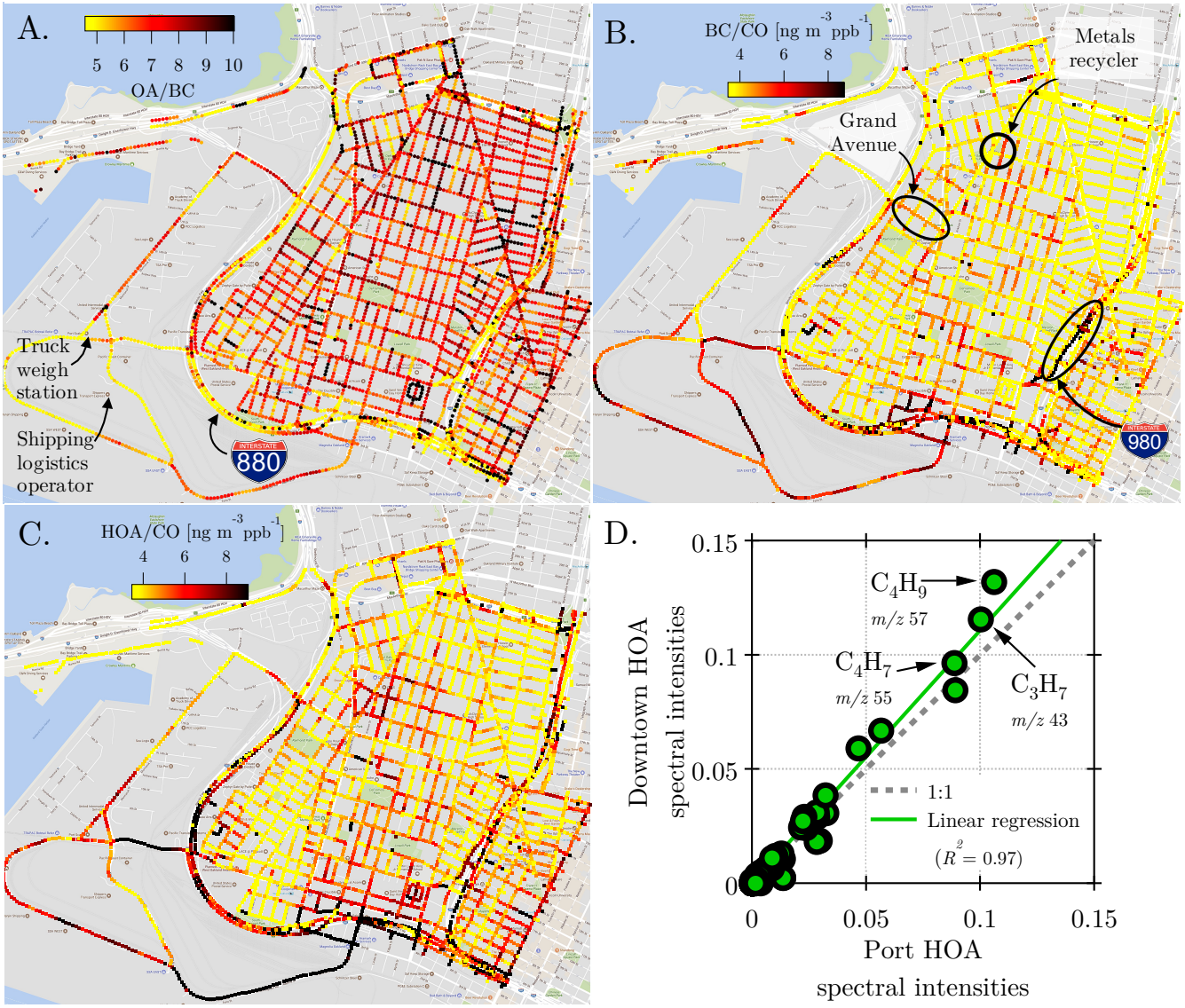

Figure 9. Fine-scale maps of (a) OA/BC (unitless), (b) BC/CO and (c) HOA/CO. Subfigure (d) shows similarity between the HOA factors identified by factorization of Port-only and downtown-only OA data. The two spectra are dominated by hydrocarbons (C_xH_y) and are highly similar to each other.

Figure 9A-C shows spatially-resolved OA/BC, BC/CO, and HOA/BC ratios. Because measurements were made at different sampling frequencies, we generate the ratios by first converting the measurements to a synthetic 1 Hz time base as described earlier. All three ratios show an influence of diesel trucks (lower OA/BC, higher BC/CO and HOA/BC) at the Port, on Interstates 880 and 980, and on truck routes that connect I-880 to the Port. The absolute concentrations of BC are also elevated in these areas (Figure S20). Bootstrap resampling the BC dataset shows that the measurements (especially in Port) have a considerable positive skew (Figure S21). The ratio of mean to median BC in Port is higher (1.5) than both West Oakland and downtown (1.2). Because BC concentrations are largely influenced by local sources (diesel trucks), the large amount of drayage trucks in Port likely causes the mean BC to be $\sim 8\%$ higher than downtown, even though median BC in downtown is $\sim 7\%$ higher than Port.

All three ratios suggest less diesel influence in West Oakland and downtown than in Port. BC/CO ratios in the Port are generally 6-8 ng m^{-3} ppb^{-1}, whereas much of West Oakland and downtown have BC/CO ~ 4 ng m^{-3} ppb^{-1}. Some hotspots of BC/CO appear in industrial parts of West Oakland, including (a) an area near a metals recycling facility in West Oakland highlighted by Apte et al. (2017) as a location with high diesel traffic and (b) a part of Grand Avenue which is also a truck route. A hotspot of BC/CO also appears on, and downwind of, I-980 in downtown.

The HOA/CO ratio paints a similar, but not identical picture as the BC/CO ratio. West Oakland and downtown have lower HOA/CO than the Port, suggesting less diesel truck influence. However, downtown has higher HOA/CO than West Oakland. Since gasoline cars appear to be the major traffic source in West Oakland and downtown, we would expect a similar HOA/CO ratio in these areas. However, several factors may contribute to the higher HOA/CO in downtown: (a) the downtown and West Oakland fleets are likely not identical (e.g., more diesel buses in downtown), (b) differences in driving mode, with more stop-and-go driving in downtown than West Oakland, and (c) larger contribution of background CO to the total measured CO in West Oakland.

The overall picture painted by Figure 9A-C is that the Port is more impacted by diesel vehicle emissions than downtown and West Oakland. Downtown has high HOA (Figure S18) because of high traffic volumes, but this area seems to be dominated by gasoline vehicles with a smaller diesel contribution. The large diesel influence at the Port persists in spite of recent, aggressive efforts to upgrade the drayage truck fleet so that the majority (99%) of drayage trucks now have diesel particulate filters (Preble et al., 2015). As shown by Dallmann et al. (2011) and Preble et al. (2015), overall BC emissions from the Port truck fleet fell by $\sim 75\%$ between 2010 and 2013, suggesting that HOA and BC concentrations at the Port were higher in the past. Further reductions in BC and HOA at the Port could be achieved by addressing high emitters; measurements by Preble et al. (2018) in 2015 showed that 7% of the drayage truck fleet at the Port accounted for 65% of the total emitted BC because the diesel particulate filters on these trucks were failing.

Since the vehicle fleet appears to be significantly different between Downtown and Port, we attempted to derive separate HOA factors for these two areas as a means to directly quantify gasoline versus diesel emissions using the AMS. We isolated Port OA data from downtown OA data and factorized them separately using PMF. The HOA factors identified for Port and downtown nearly identical ($R^2 = 0.97$; Figure 9D). This is likely due to a combination of similar emissions (HOA from gasoline and diesel

excessive fragmentation upon ionization in the AMS. The similarity in the Port and Downtown HOA factors makes it essentially impossible to distinguish HOA emitted by diesel trucks from HOA emitted by gasoline cars.

3.5 Elemental analysis of bulk and factor OA

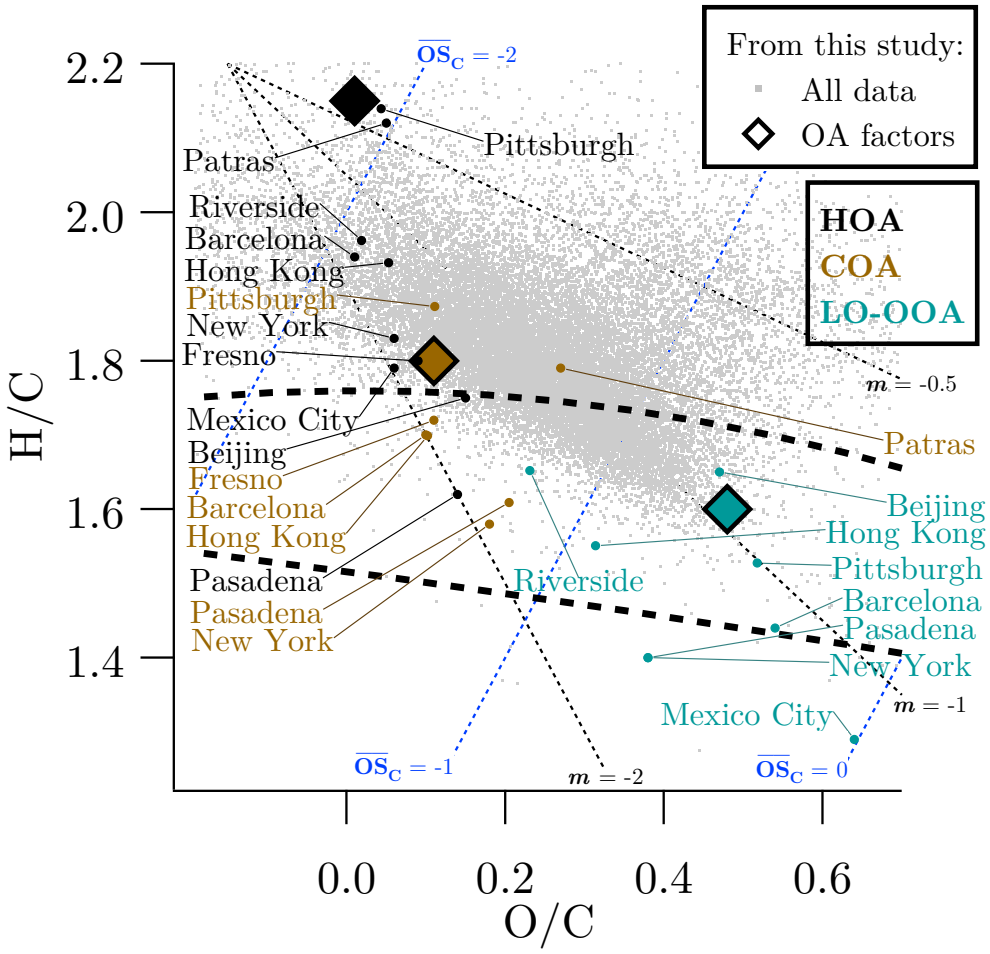

Figure 10. The Van Krevelen plane. Gray points represent all OA measurements in this study. Diamonds represent OA factors identified in this study. For reference, placement of OA factors from other ambient measurements are shown: Pittsburgh ~~(Gu et al. *in prep.*)~~(Gu et al., 2018), Patras, Greece (Kaltsonoudis et al., 2017), Riverside, CA (Docherty et al., 2011), Barcelona (Mohr et al., 2012), Hong Kong (Lee et al., 2015), New York, NY (Sun et al., 2011), Fresno, CA (Ge et al., 2012), Mexico City (Decarlo et al., 2010), Beijing (Hu et al., 2016) and Pasadena, CA (Hayes et al., 2013). Different oxygenation pathways are shown by the black dotted lines. Dotted blue lines are isopleths for average carbon oxidation states ($\overline{OS}_C = 2 \times O/C - H/C$). The region of ambient oxygenated OA measurements, as reported by Ng et al. (2011), is shown between the dashed curves.

In this section, we investigate the measured elemental ratios (H/C and O/C) of OA using a Van Krevelen (VK) diagram. Figure 10 shows all bulk OA data from this study (gray dots). Only 21% of the bulk data fall inside the typical ambient range of OOA measurements (Ng et al., 2011), while the remaining data are on the less oxygenated side of this range. This indicates a dominant presence of highly reduced, primary OA in Oakland. This finding contrasts with the measurements made in other urban areas. For instance, almost all of the bulk OA measurements made in Pasadena, CA were either inside or below (i.e., more oxygenated than) this ambient OOA region (Ortega et al., 2016). This finding is consistent with the large contribution of primary OA in Oakland (Figures 4 and 5) and can be partially explained by the overall spatial proximity of ≤ 1 km of all points inside the domain to the nearest highway (Apte et al., 2017). Primary emissions are thus of more importance in Oakland than other urban areas.

Figure 10 also shows that the cluster of bulk OA data from this study aligns with the -1 slope line (slope of linear fit = -1.003, not shown; Pearson's R = 0.62). Previous studies have used VK slopes to determine if the processing of ambient OA is dominated by chemical (e.g., oxygenation) or physical (e.g., external mixing of air masses) mechanisms. By isolating chemical processing of Pasadena OA in an oxidation flow reactor, Ortega et al. (2016) showed that chemical processing shifts OA on the VK plane along a shallow slope of ~ -0.7. A similar slope was observed by Liu et al. (2018) by chemical processing of Beijing OA in an oxidation flow reactor. Similarly, Presto et al. (2014) measured a slope of ~ -0.5 for oxidation of fresh gasoline and diesel exhaust in a smog chamber. By comparing OA measurements in Riverside, CA with those in Pasadena, Hayes et al. (2013) hypothesized that the ~~HOA-to-SV-OOA~~ HOA-to-LO-OOA transformation in Riverside occurred with a steeper VK slope ($m = -1.1$) due to the physical mixing of highly reduced ($\overline{\text{OS}}_\text{C} = 2\times\text{O/C}-\text{H/C} = -1.92$; Kroll et al., 2011; Canagaratna et al., 2015), HOA-rich air masses with OOA-rich air masses in Riverside.

Figure 10 also plots the HOA, COA and ~~SV-OOA~~ LO-OOA factors identified in this study on the VK plane. For reference, similar factors are shown from ambient measurements reported in prior publications. As expected, reduced factors corresponding to primary emissions (HOA and COA) occur closer towards the top-left corner of the VK plane, while the ~~SV-OOA~~ LO-OOA factors occur closer towards the bottom-right corner. With the exception of Pittsburgh and Patras, HOA in Oakland is more chemically reduced ($\overline{\text{OS}}_\text{C}$ = -2.13) compared to HOA in other locations (average $\overline{\text{OS}}_\text{C} \sim$ -1.7). That the composition of HOA in Oakland is more reduced, as well as the overall slope for all OA measurements in Oakland is $\sim$ -1, suggests that external mixing of highly reduced, HOA-rich air masses with OOA-rich air masses is an important processing mechanism in Oakland. This is also consistent with the recent findings of Ye et al. (2018) via single-particle mass spectrometry in Pittsburgh, PA; particle mixing state shifts from internal to external with $\sim$ km-scale proximity to urban sources. It is also worth noting in Figure 10 that the HOA measurements that are more chemically-reduced (Oakland, Pittsburgh and Patras) were performed in the past 5 years, compared to the other measurements that were made earlier ($\sim$ 10 years ago). This suggests a change in the chemical composition of vehicular emissions over the past decade.

Finally, this VK analysis also reinforces the choice of a 3-factor PMF solution in this study. In Figure S15, the 3- and 4-factor PMF solutions are compared on the VK plane, along with other reference data as already described in Figure 10. The HOA and COA markers do not change their position on the VK plane between the 3- and 4-factor solutions. This is consistent with the robustness of HOA and COA mass fractions to the choice of PMF solutions, as described earlier and shown in Figure S14.

However, the ~~SV-OOA~~ LO-OOA factor in the 3-factor solution is split into a highly oxygenated ~~LV-OOA~~ MO-OOA factor and a fourth, unknown factor. We explained earlier that the 4-factor solution is an artificial splitting of the 3-factor solution. The placement of these factors on the VK planes is consistent with this explanation. The ~~LV-OOA~~ MO-OOA factor occurs in the far bottom-right corner, where there are no bulk OA data. The fourth OA factor coincides with the center of mass of the bulk OA data cluster, likely because the artificial splitting of the ~~SV-OOA~~ LO-OOA factor is done with the constraint of minimizing residuals (Q/Q_{exp}). Further, the ~~SV-OOA, LV-OOA~~ LO-OOA, MO-OOA and the unknown factor all fall on the same $m = 1$ dotted line. Thus, from a strictly mathematical standpoint, this solution offers no new information, given that the ~~LV-OOA~~ MO-OOA and the unknown factor average along the $m = 1$ line to form the ~~SV-OOA~~ LO-OOA factor.

4 Summary and conclusions

Having one of U.S.'s largest shipping ports, the air quality in Oakland has been historically impacted by shipping-related activities such as presence of ships burning high-sulfur fuel and drayage trucks driving through the directly adjacent residential neighborhood (Fisher et al., 2006; Fujita et al., 2013). In the past decade, regulations on ~~drayage trucks and~~ ship fuel usage have dramatically reduced emissions (Tao et al., 2013; Dallmann et al., 2011; Preble et al., 2015). ~~Findings of this study are consistent with these previous studies regarding the substantially improved air quality in Oakland. However, the port is not~~ Further, more than 70% of the ~~only source of emissions that could impact~~ ships at the Port now utilize shore power provision and thus do not idle their engines. It is thus reasonable to expect that the influence of ship emissions on the air quality in Oakland ~~. The city also has~~ has substantially reduced after the measurements of Tao et al. (2013). Enforced installation of diesel particulate filters on drayage trucks has also significantly reduced truck emissions at the Port Dallmann et al. (2011); Preble et al. (2015), although a recent finding by Preble et al. (2018) has raised concern about the exhaustion of these filters and the resultant increase in truck emissions.

In addition to the Port, Oakland also has a central business district ("downtown") that has activities such as domestic vehicular traffic and cooking, similar to other urban areas. ~~Therefore, urban~~ Urban downtowns are also a prominent source of organic aerosols (OA; Mohr et al., 2015), which make up a dominant part of particulate matter (PM). Since the residential West Oakland neighborhood falls in the middle of the port and downtown, it is important from a health exposure perspective to determine the spatial variability of pollutants within the city and to determine which of these two area sources drive spatial variability in PM.

The objective of this study was to examine the spatial and temporal patterns in pollutants impacting the air quality in Oakland through mobile sampling in an instrumented van. Organic aerosol (OA) contributes the largest fraction ($\sim$ 50%) of PM_1 mass. We find that primary emissions from cooking (COA) and vehicles (HOA) as well as secondary OA (~~SV-OOA~~LO-OOA) contribute to the spatial variation within Oakland. Key findings are:

1. Organic aerosol is the dominant component of PM_1 (OA; $\sim$ 50%), and its contribution is roughly twice that of sulfate (23%). This finding is consistent with the that of Tao et al. (2013), who also showed that the enforcement of low-sulfur fuel usage in ships has successfully reduced the amounts of particulate-phase SO_4^{2-} in the local PM in Oakland.

2. In downtown, concentrations of primary OA are higher than secondary OA. The dominant source of these primary OA emissions shifts diurnally between cooking and vehicles: pre-10 AM fresh emissions are from vehicles, but cooking emissions contribute dominantly to OA after lunchtime. ~~Further, by investigating the ratio of OA emitted from vehicles to~~

3. While it is challenging to mathematically apportion traffic-emitted OA between drayage trucks and cars, we use ratios of OA and black carbon (BC; particulate matter emitted typically from diesel combustion in trucks) ~~, we~~ to CO and show that drayage truck emissions ~~do affect the spatial variability of OA in space (Port) and time (afternoon,~~ have an important effect on the concentrations of OA and BC at the Port, especially when truck traffic typically peaks ~~).~~ in the afternoon. However, cars seem to be the dominant source of traffic emissions in Downtown and West Oakland.

4. Secondary OA (SOA) also exhibits spatial variability similar to primary OA. ~~SV-OOA~~ LO-OOA concentrations are higher in downtown, likely because a combination of various factors (poor ventilation of air masses in street canyon, higher emissions of SOA precursors, higher OH concentrations) result in downtown being a microenvironment with high photochemical activity.

5. Overall chemical composition of OA in Oakland is more chemically-reduced relative to that reported in studies in several other locations. Especially, HOA in Oakland is more reduced than other locations. This reflects the importance of primary emissions in Oakland. Further, by comparing measurements from other studies, we show that the chemical composition of HOA has likely become more reduced over the last decade. Lastly, external mixing of air masses with contrasting pollutant concentrations plays an important role in the processing of these chemically-reduced emissions.

These findings have important implications for population exposure studies because urban downtowns tend to have a concentrated presence of workplaces, resulting in people being exposed to these elevated pollutant concentrations for $\sim$ 8 h (typical work day duration) ~~everyday~~every day. These findings are experimentally shown for Oakland as a case city, which has unique elements (oceanic winds mixing with urban emissions, presence of a major port) that likely have a unique influence on the intra-city patterns in its air quality. However, Oakland also has elements that are fairly typical of urban areas (e.g., downtown with high cooking and vehicular emissions). The findings of this study are thus likely applicable to other urban areas as well, because the pollutants we find contributing the most to OA variability, both of primary and secondary origin, are ubiquitous in other urban locations.

Author contributions. RUS, ESR and PG collected data. RUS performed data analysis with input from all co-authors on the interpretation of results. RUS and AAP wrote the manuscript with significant input from ALR. ALR, JSA and AAP designed the research.

Competing interests. The authors declare no competing financial interest.

Acknowledgements. This research was funded by Environmental Defense Fund (EDF) and NSF grant number AGS1543786.

This publication was developed under Assistance Agreement No. RD83587301 awarded by the U.S. Environmental Protection Agency. This work has not been formally reviewed by the funding agencies. The views expressed in this document are solely those of the authors and do not necessarily reflect those of the funding agencies. EPA does not endorse any products or commercial services mentioned in this publication.

We thank Sarah Seraj (UT Austin) for her assistance with data collection; Thomas Kirchstetter, Chelsea Preble and Julien Caubel (Lawrence Berkeley National Lab) for assistance with calibration instrumentation.

References

Alameda County: Alameda County Data Sharing Initiative, https://data.acgov.org/browse?category=GeospatialData{&}anonymous=true{&}q=street{&}sortBy=relevance, 2017.

Apte, J. S., Marshall, J. D., Cohen, A. J., and Brauer, M.: Addressing Global Mortality from Ambient $PM_{2.5}$, Environmental Science and Technology, 49, 8057–8066, https://doi.org/10.1021/acs.est.5b01236, http://dx.doi.org/10.1021/acs.est.5b01236, 2015.

Apte, J. S., Messier, K. P., Gani, S., Brauer, M., Kirchstetter, T. W., Lunden, M. M., Marshall, J. D., Portier, C. J., Vermeulen, R. C. H., and Hamburg, S. P.: High-Resolution Air Pollution Mapping with Google Street View Cars : Exploiting Big Data, Environmental Science & Technology, https://doi.org/10.1021/acs.est.7b00891, http://dx.doi.org/10.1021/acs.est.7b00891, 2017.

BAAQMD: Interactive Data Maps, http://www.baaqmd.gov/research-and-data/interactive-data-maps, 2018.

Ban-Weiss, G. A., McLaughlin, J. P., Harley, R. A., Lunden, M. M., Kirchstetter, T. W., Kean, A. J., Strawa, A. W., Stevenson, E. D., and Kendall, G. R.: Long-term changes in emissions of nitrogen oxides and particulate matter from on-road gasoline and diesel vehicles, Atmospheric Environment, 42, 220–232, https://doi.org/10.1016/j.atmosenv.2007.09.049, 2008.

Brantley, H. L., Hagler, G. S. W., Kimbrough, E. S., Williams, R. W., Mukerjee, S., and Neas, L. M.: Mobile air monitoring data-processing strategies and effects on spatial air pollution trends, Atmospheric Measurement Techniques, 7, 2169–2183, https://doi.org/10.5194/amt-7-2169-2014, 2014.

Canagaratna, M. R., Onasch, T. B., Wood, E. C., Herndon, S. C., Jayne, J. T., Cross, E. S., Miake-Lye, R. C., Kolb, C. E., and Worsnop, D. R.: Evolution of vehicle exhaust particles in the atmosphere, Journal of the Air and Waste Management Association, 60, 1192–1203, https://doi.org/10.3155/1047-3289.60.10.1192, 2010.

Canagaratna, M. R., Jimenez, J. L., Kroll, J. H., Chen, Q., Kessler, S. H., Massoli, P., and Ruiz, L. H.: Elemental ratio measurements of organic compounds using aerosol mass spectrometry : characterization , improved calibration , and implications, pp. 253–272, https://doi.org/10.5194/acp-15-253-2015, http://dx.doi.org/10.5194/acp-15-253-2015, 2015.

CARB: California Air Resource Board (CARB): Final Regulation Order - Fuel Sulfur and Other Operational Requirements for Ocean-Going Vessels Within California Waters and 24 Nautical Miles of the California Baseline, https://www.arb.ca.gov/regact/2008/fuelogv08/fro13.pdf, 2009.

CARB: California Air Resource Board (CARB): Overview of the Statewide Drayage Truck Regulation, https://www.arb.ca.gov/msprog/onroad/porttruck/regfactsheet.pdf, 2011.

Choi, W., He, M., Barbesant, V., Kozawa, K. H., Mara, S., Winer, A. M., and Paulson, S. E.: Prevalence of wide area impacts downwind of freeways under pre-sunrise stable atmospheric conditions, Atmospheric Environment, 62, 318–327, https://doi.org/10.1016/j.atmosenv.2012.07.084, http://dx.doi.org/10.1016/j.atmosenv.2012.07.084, 2012.

City of Oakland: City of Oakland Planning and Zoning, http://www2.oaklandnet.com/government/o/PBN/OurOrganization/PlanningZoning/s/codes/index.htm, 2017.

Crippa, M., El Haddad, I., Slowik, J. G., Decarlo, P. F., Mohr, C., Heringa, M. F., Chirico, R., Marchand, N., Sciare, J., Baltensperger, U., and Prévôt, A. S.: Identification of marine and continental aerosol sources in Paris using high resolution aerosol mass spectrometry, Journal of Geophysical Research Atmospheres, 118, 1950–1963, https://doi.org/10.1002/jgrd.50151, ~~2013.~~ 2013a.

Crippa, M., Decarlo, P. F., Slowik, J. G., Mohr, C., Heringa, M. F., Chirico, R., Poulain, L., Freutel, F., Sciare, J., Cozic, J., Di Marco, C. F., Elsasser, M., Nicolas, J. B., Marchand, N., Abidi, E., Wiedensohler, A., Drewnick, F., Schneider, J., Borrmann, S., Nemitz, E., Zimmermann, R., Jaffrezo, J. L., Prévôt, A. S., and Baltensperger, U.: Wintertime aerosol chemical composition and source apportionment

of the organic fraction in the metropolitan area of Paris, Atmospheric Chemistry and Physics, 13, 961–981, https://doi.org/10.5194/acp-13-961-2013, 2013b.

Dallmann, T. R., Harley, R. A., and Kirchstetter, T. W.: Effects of diesel particle filter retrofits and accelerated fleet turnover on drayage truck emissions at the port of Oakland, Environmental Science and Technology, 45, 10 773–10 779, https://doi.org/10.1021/es202609q, http://dx.doi.org/10.1021/es202609q, 2011.

Dallmann, T. R., Kirchstetter, T. W., Demartini, S. J., and Harley, R. A.: Quantifying on-road emissions from gasoline-powered motor vehicles: Accounting for the presence of medium- and heavy-duty diesel trucks, Environmental Science and Technology, 47, 13 873–13 881, , 2013.

Decarlo, P. F., Kimmel, J. R., Trimborn, A., Northway, M., Jayne, J. T., Aiken, A. C., Gonin, M., Fuhrer, K., Horvath, T., Docherty, K. S., Worsnop, D. R., and Jimenez, J. L.: Field-Deployable, High-Resolution, Time-of-Flight Aerosol Mass Spectrometer, Analytical Chemistry, 78, 8281–8289, https://doi.org/8410.1029/2001JD001213.Analytical, http://www.agu.org/pubs/crossref/2003/2001JD001213.shtml, 2006.

Decarlo, P. F., Ulbrich, I. M., Crounse, J., De Foy, B., Dunlea, E. J., Aiken, A. C., Knapp, D., Weinheimer, A. J., Campos, T., Wennberg, P. O., and Jimenez, J. L.: Investigation of the sources and processing of organic aerosol over the Central Mexican Plateau from aircraft measurements during MILAGRO, Atmospheric Chemistry and Physics, 10, 5257–5280, https://doi.org/10.5194/acp-10-5257-2010, http://dx.doi.org/10.5194/acp-10-5257-2010, 2010.

Docherty, K. S., Aiken, A. C., Huffman, J. A., Ulbrich, I. M., Decarlo, P. F., Sueper, D., Worsnop, D. R., Snyder, D. C., Peltier, R. E., Weber, R. J., Grover, B. D., Eatough, D. J., Williams, B. J., Goldstein, A. H., Ziemann, P. J., and Jimenez, J. L.: The 2005 Study of Organic Aerosols at Riverside (SOAR-1): Instrumental intercomparisons and fine particle composition, Atmospheric Chemistry and Physics, 11, 12 387–12 420, https://doi.org/10.5194/acp-11-12387-2011, http://dx.doi.org/10.5194/acp-11-12387-2011, 2011.

Donahue, N. M., Kroll, J. H., Pandis, S. N., and Robinson, A. L.: A two-dimensional volatility basis set-Part 2: Diagnostics of organic-aerosol evolution, Atmospheric Chemistry and Physics, 12, 615–634, https://doi.org/10.5194/acp-12-615-2012, 2012.

Elser, M., Bozzetti, C., El-Haddad, I., Maasikmets, M., Teinemaa, E., Richter, R., Wolf, R., Slowik, J. G., Baltensperger, U., and Prevot, A. S.: Urban increments of gaseous and aerosol pollutants and their sources using mobile aerosol mass spectrometry measurements, Atmospheric Chemistry and Physics, 16, 7117–7134, https://doi.org/10.5194/acp-16-7117-2016, http://dx.doi.org/10.5194/acp-16-7117-2016, 2016.

Enroth, J., Saarikoski, S., Niemi, J., Kousa, A., Ježek, I., Močnik, G., Carbone, S., Kuuluvainen, H., Rönkkö, T., Hillamo, R., and Pirjola, L.: Chemical and physical characterization of traffic particles in four different highway environments in the Helsinki metropolitan area, Atmospheric Chemistry and Physics, 16, 5497–5512, https://doi.org/10.5194/acp-16-5497-2016, 2016.

Ferin, J., Oberdörster, G., and Penney, D. P.: Pulmonary Retention of Ultrafine and Fine Particles in Rats, American Journal of Respiratory Cell and Molecular Biology, 6, 535–542, https://doi.org/10.1165/ajrcmb/6.5.535, http://www.atsjournals.org/doi/abs/10.1165/ajrcmb/6.5.535, 1992.

Finlayson-Pitts, B. J. and Pitts, J. N.: in: Chemistry of the Upper and Lower Atmosphere, edited by Finlayson-Pitts, B. J. and Pitts, J. N., pp. 264 – 293, Academic Press, San Diego, https://doi.org/https://doi.org/10.1016/B978-012257060-5/50009-5, http://www.sciencedirect.com/science/article/pii/B9780122570605500095, 2000.

Fisher, J. B., Kelly, M., and Romm, J.: Scales of environmental justice: Combining GIS and spatial analysis for air toxics in West Oakland, California, Health and Place, 12, 701–714, https://doi.org/10.1016/j.healthplace.2005.09.005, http://dx.doi.org/10.1016/j.healthplace.2005.09.005, 2006.

Fujita, E. M., Campbell, D. E., Patrick Arnott, W., Lau, V., and Martien, P. T.: Spatial variations of particulate matter and air toxics in communities adjacent to the Port of Oakland, Journal of the Air and Waste Management Association, 63, 1399–1411, https://doi.org/10.1080/10962247.2013.824393, http://dx.doi.org/10.1080/10962247.2013.824393, 2013.

Ge, X., Setyan, A., Sun, Y., and Zhang, Q.: Primary and secondary organic aerosols in Fresno, California during wintertime: Results from high resolution aerosol mass spectrometry, Journal of Geophysical Research Atmospheres, 117, 1–15, https://doi.org/10.1029/2012JD018026, http://dx.doi.org/10.1029/2012JD018026, 2012.

Giuliano, G. and O'Brien, T.: Reducing port-related truck emissions: The terminal gate appointment system at the Ports of Los Angeles and Long Beach, Transportation Research Part D: Transport and Environment, 12, 460–473, https://doi.org/10.1016/j.trd.2007.06.004, 2007.

Goldstein, A. H. and Galbally, I. E.: Known and unexplored organic constituents in the earth's atmosphere, Environmental Science and Technology, 41, 1514–1521, https://doi.org/10.1021/es072476p, http://dx.doi.org/10.1021/es072476p, 2007.

Gordon, T. D., Tkacik, D. S., Presto, A. A., Zhang, M., Jathar, S. H., Nguyen, N. T., Massetti, J., Truong, T., Cicero-Fernandez, P., Maddox, C., Rieger, P., Chattopadhyay, S., Maldonado, H., Maricq, M. M., and Robinson, A. L.: Primary gas- and particle-phase emissions and secondary organic aerosol production from gasoline and diesel off-road engines, Environmental Science and Technology, 47, 14 137–14 146, https://doi.org/10.1021/es403556e, 2013.

Gu, P., Li, H. Z., Ye, Q., Robinson, E. S., Apte, J. S., Robinson, A. L., and Presto, A. A.: ~~Carbonaceous Sources Drive Intra-City Variability of Aerosol Exposure, Submitted,~~ Intra-city variability of PM exposure is driven by carbonaceous sources and correlated with land use variables, Environmental Science & Technology, Accepted, https://doi.org/10.1021/acs.est.8b03833, https://doi.org/10.1021/acs.est.8b03833, 2018.

Hallquist, M., Wenger, J. C., Baltensperger, U., Rudich, Y., Simpson, D., Claeys, M., Dommen, J., Donahue, N. M., George, C., Goldstein, a. H., Hamilton, J. F., Herrmann, H., Hoffmann, T., Iinuma, Y., Jang, M., Jenkin, M. E., Jimenez, J. L., Kiendler-Scharr, a., Maenhaut, W., McFiggans, G., Mentel, T. F., Monod, a., Prevot, a. S. H., Seinfeld, J. H., Surratt, J. D., Szmigielski, R., and Wildt, J.: The formation, properties and impact of secondary organic aerosol: current and emerging issues, Atmos. Chem. Phys., 9, 5155–5236, https://doi.org/10.5194/acp-9-5155-2009, http://dx.doi.org/10.5194/acp-9-5155-2009, 2009.

Hayes, P. L., Ortega, A. M., Cubison, M. J., Froyd, K. D., Zhao, Y., Cliff, S. S., Hu, W. W., Toohey, D. W., Flynn, J. H., Lefer, B. L., Grossberg, N., Alvarez, S., Rappenglück, B., Taylor, J. W., Allan, J. D., Holloway, J. S., Gilman, J. B., Kuster, W. C., De Gouw, J. A., Massoli, P., Zhang, X., Liu, J., Weber, R. J., Corrigan, A. L., Russell, L. M., Isaacman, G., Worton, D. R., Kreisberg, N. M., Goldstein, A. H., Thalman, R., Waxman, E. M., Volkamer, R., Lin, Y. H., Surratt, J. D., Kleindienst, T. E., Offenberg, J. H., Dusanter, S., Griffith, S., Stevens, P. S., Brioude, J., Angevine, W. M., and Jimenez, J. L.: Organic aerosol composition and sources in Pasadena, California, during the 2010 CalNex campaign, Journal of Geophysical Research Atmospheres, 118, 9233–9257, https://doi.org/10.1002/jgrd.50530, http://dx.doi.org/10.1002/jgrd.50530, 2013.

Hildebrandt, L., Engelhart, G. J., Mohr, C., Kostenidou, E., Lanz, V. A., Bougiatioti, A., Decarlo, P. F., Prevot, A. S. H., Baltensperger, U., Mihalopoulos, N., Donahue, N. M., and Pandis, S. N.: Aged organic aerosol in the Eastern Mediterranean: The Finokalia Aerosol Measurement Experiment-2008, Atmospheric Chemistry and Physics, 10, 4167–4186, https://doi.org/10.5194/acp-10-4167-2010, http://dx.doi.org/10.5194/acp-10-4167-2010, 2010.

Hoek, G., Meliefste, K., Cyrys, J., Lewné, M., Bellander, T., Brauer, M., Fischer, P., Gehring, U., Heinrich, J., Van Vliet, P., and Brunekreef, B.: Spatial variability of fine particle concentrations in three European areas, Atmospheric Environment, 36, 4077–4088, https://doi.org/10.1016/S1352-2310(02)00297-2, 2002.

Hu, W., Hu, M., Hu, W., Jimenez, J. L., Yuan, B., Chen, W., Wang, M., Wu, Y., Chen, C., Wang, Z., Peng, J., Zeng, L., and Shao, M.: Chemical composition, sources, and aging process of submicron aerosols in Beijing: Contrast between summer and winter, pp. 1955–1977, https://doi.org/10.1002/2015JD024020.Received, http://dx.doi.org/10.1002/2015JD024020.Received, 2016.

Jayne, J. T., Leard, D. C., Zhang, X. F., Davidovits, P., Smith, K. a., Kolb, C. E., and Worsnop, D. R.: Development of an aerosol mass spectrometer for size and composition analysis of submicron particles, Aerosol Science and Technology, 33, 49–70, https://doi.org/10.1080/027868200410840, http://dx.doi.org/10.1080/027868200410840, 2000.

Jimenez, J. L., Canagaratna, M. R., Donahue, N. M., Prevot, A. S. H., Zhang, Q., Kroll, J. H., DeCarlo, P. F., Allan, J. D., Coe, H., Ng, N. L., Aiken, A. C., Docherty, K. S., Ulbrich, I. M., Grieshop, A. P., Robinson, A. L., Duplissy, J., Smith, J. D., Wilson, K. R., Lanz, V. A., Hueglin, C., Sun, Y. L., Tian, J., Laaksonen, A., Raatikainen, T., Rautiainen, J., Vaattovaara, P., Ehn, M., Kulmala, M., Tomlinson, J. M., Collins, D. R., Cubison, M. J., Dunlea, E. J., Huffman, J. A., Onasch, T. B., Alfarra, M. R., Williams, P. I., Bower, K., Kondo, Y., Schneider, J., Drewnick, F., Borrmann, S., Weimer, S., Demerjian, K., Salcedo, D., Cottrell, L., Griffin, R., Takami, A., Miyoshi, T., Hatakeyama, S., Shimono, A., Sun, J. Y., Zhang, Y. M., Dzepina, K., Kimmel, J. R., Sueper, D., Jayne, J. T., Herndon, S. C., Trimborn, A. M., Williams, L. R., Wood, E. C., Middlebrook, A. M., Kolb, C. E., Baltensperger, U., and Worsnop, D. R.: Evolution of organic aerosols in the atmosphere, Science, 326, 1525–1529, http://www.scopus.com/inward/record.url?eid=2-s2.0-72149091509%7B%5C&%7DpartnerID=40%7B%5C&%7Dmd5=659a09933e64bfec92e2296514dfa504, 2009.

Kaltsonoudis, C., Kostenidou, E., Louvaris, E., Psichoudaki, M., Tsiligiannis, E., Florou, K., Liangou, A., and Pandis, S. N.: Characterization of fresh and aged organic aerosol emissions from meat charbroiling, Atmospheric Chemistry and Physics, 17, 7143–7155, https://doi.org/10.5194/acp-17-7143-2017, http://dx.doi.org/10.5194/acp-17-7143-2017, 2017.

Knoderer, C., Nguyen, D., Alrick, D., and Hoag, K.: 2015 Air Monitoring Network Plan, Tech. rep., Bay Area Air Quality Management District, San Francisco, CA, http://www.baaqmd.gov/{~}/media/files/technical-services/2015{_}network{_}plan-pdf.pdf?la=en, 2016.

Kroll, J. H., Donahue, N. M., Jimenez, J. L., Kessler, S. H., Canagaratna, M. R., Wilson, K. R., Altieri, K. E., Mazzoleni, L. R., Wozniak, A. S., Bluhm, H., Mysak, E. R., Smith, J. D., Kolb, C. E., and Worsnop, D. R.: Carbon oxidation state as a metric for describing the chemistry of atmospheric organic aerosol, Nature Chemistry, 3, 133–139, https://doi.org/10.1038/nchem.948, http://dx.doi.org/10.1038/nchem.948, 2011.

Lee, B. P., Li, Y. J., Yu, J. Z., Louie, P. K. K., and Chan, C. K.: Characteristics of submicron particulate matter at the urban roadside in downtown Hong Kong—Overview of 4 months of continuous high-resolution aerosol mass spectrometer measurements, pp. 1–19, https://doi.org/10.1002/2015JD023311.Received, http://dx.doi.org/10.1002/2015JD023311.Received, 2015.

Li, H. Z., Dallmann, T. R., Gu, P., Presto, A. A., and Edu, A. C.: Application of mobile sampling to investigate spatial variation in fine particle composition Application of mobile sampling to investigate spatial, Atmospheric Environment, 142, 71–82, https://doi.org/10.1016/j.atmosenv.2016.07.042, http://dx.doi.org/10.1016/j.atmosenv.2016.07.042, ~~2016.~~ 2016a.

Li, H. Z., Dallmann, T. R., Li, X., Gu, P., and Presto, A. A.: Urban organic aerosol exposure: Spatial variations in composition and source impacts, Environmental Science and Technology, https://doi.org/10.1021/acs.est.7b03674, http://dx.doi.org/10.1021/acs.est.7b03674, 2018.

Li, X., Dallmann, T. R., May, A. A., Tkacik, D. S., Lambe, A. T., Jayne, J. T., Croteau, P. L., and Presto, A. A.: Gas-Particle Partitioning of Vehicle Emitted Primary Organic Aerosol Measured in a Traffic Tunnel, Environmental Science and Technology, 50, 12 146–12 155, https://doi.org/10.1021/acs.est.6b01666, 2016b.

Liu, J., Chu, B., Chen, T., Liu, C., Wang, L., Bao, X., and He, H.: Secondary Organic Aerosol Formation from Ambient Air at an Urban Site in Beijing: Effects of OH Exposure and Precursor Concentrations, Environmental Science and Technology, 52, 6834–6841, https://doi.org/10.1021/acs.est.7b05701, 2018.

May, A. A., Nguyen, N. T., Presto, A. A., Gordon, T. D., Lipsky, E. M., Karve, M., Gutierrez, A., Robertson, W. H., Zhang, M., Brandow, C., Chang, O., Chen, S., Cicero-Fernandez, P., Dinkins, L., Fuentes, M., Huang, S. M., Ling, R., Long, J., Maddox, C., Massetti, J., McCauley, E., Miguel, A., Na, K., Ong, R., Pang, Y., Rieger, P., Sax, T., Truong, T., Vo, T., Chattopadhyay, S., Maldonado, H., Maricq, M. M., and Robinson, A. L.: Gas- and particle-phase primary emissions from in-use, on-road gasoline and diesel vehicles, Atmospheric Environment, 88, 247–260, https://doi.org/10.1016/j.atmosenv.2014.01.046, http://dx.doi.org/10.1016/j.atmosenv.2014.01.046, 2014.

Middlebrook, A. M., Bahreini, R., Jimenez, J. L., and Canagaratna, M. R.: Evaluation of Composition-Dependent Collection Efficiencies for the Aerodyne Aerosol Mass Spectrometer using Field Data, Aerosol Science and Technology, 46, 258–271, https://doi.org/10.1080/02786826.2011.620041, http://dx.doi.org/10.1080/02786826.2011.620041, 2012.

Miyakawa, T., Takegawa, N., and Kondo, Y.: Removal of sulfur dioxide and formation of sulfate aerosol in Tokyo, Journal of Geophysical Research Atmospheres, 112, 1–13, https://doi.org/10.1029/2006JD007896, 2007.

Mohr, C., Huffman, J. A., Cubison, M. J., Aiken, A. C., Docherty, K. S., Kimmel, J. R., Ulbrich, I. M., Hannigan, M., and Jimenez, J. L.: Characterization of primary organic aerosol emissions from meat cooking, trash burning, and motor vehicles with high-resolution aerosol mass spectrometry and comparison with ambient and chamber observations, Environmental Science and Technology, 43, 2443–2449, https://doi.org/10.1021/es8011518, http://dx.doi.org/10.1021/es8011518, 2009.

Mohr, C., DeCarlo, P. F., Heringa, M. F., Chirico, R., Slowik, J. G., Richter, R., Reche, C., Alastuey, A., Querol, X., Seco, R., Penuelas, J., Jimenez, J. L., Crippa, M., Zimmermann, R., Baltensperger, U., and Prevot, A. S. H.: Identification and quantification of organic aerosol from cooking and other sources in Barcelona using aerosol mass spectrometer data, Atmos. Chem. Phys., 12, 1649–1665, https://doi.org/10.5194/acp-12-1649-2012, http://www.atmos-chem-phys.net/12/1649/2012/{%}5Cnhttp://www.atmos-chem-phys.net/12/1649/2012/acp-12-1649-2012.pdf, 2012.

Mohr, C., DeCarlo, P. F., Heringa, M. F., Chirico, R., Richter, R., Crippa, M., Querol, X., Baltensperger, U., and Prevot, A. S. H.: Spatial Variation of Aerosol Chemical Composition and Organic Components Identified by Positive Matrix Factorization in the Barcelona Region, Environmental Science and Technology, 49, 10 421–10 430, https://doi.org/10.1021/acs.est.5b02149, http://dx.doi.org/10.1021/acs.est.5b02149, 2015.

Myhre, G., Samset, B. H., Schultz, M. G., Balkanski, Y., Bauer, S., Berntsen, T. K., Bian, H., Bellouin, N., Chin, M., Diehl, T., Easter, R. C., Feichter, J., Ghan, S. J., Hauglustaine, D., Iversen, T., Kinne, S., Kirkeväg, A., Lamarque, J. F., Lin, G., Liu, X., Lund, M. T., Luo, G., Ma, X., van Noije, T., Penner, J. E., Rasch, P. J., Ruiz, A., Seland, Ø., Skeie, R. B., Stier, P., Takemura, T., Tsigaridis, K., Wang, P., Wang, Z., Xu, L., Yu, H., Yu, F., Yoon, J. H., Zhang, K., Zhang, H., and Zhou, C.: Radiative forcing of the direct aerosol effect from AeroCom Phase II simulations, Atmospheric Chemistry and Physics, 13, 1853–1877, https://doi.org/10.5194/acp-13-1853-2013, http://dx.doi.org/10.5194/acp-13-1853-2013, 2013.

~~Ng, N. L., Canagaratna, M. R., Zhang, Q., Jimenez, J. L., Tian, J., Ulbrich, I. M., Kroll, J. H., Docherty, K. S., Chhabra, P. S., Bahreini, R., Murphy, S. M., Seinfeld, J. H., Hildebrandt, L., Donahue, N. M., Decarlo, P. F., Lanz, V. A., Prevot, A. S., Dinar, E., Rudich, Y., and Worsnop, D. R.: Organic aerosol components observed in Northern Hemispheric datasets from Aerosol Mass Spectrometry, Atmospheric Chemistry and Physics, 10, 4625–4641, , , 2010.~~

Ng, N. L., Canagaratna, M. R., Jimenez, J. L., Chhabra, P. S., Seinfeld, J. H., and Worsnop, D. R.: Changes in organic aerosol composition with aging inferred from aerosol mass spectra, Atmospheric Chemistry and Physics, 11, 6465–6474, https://doi.org/10.5194/acp-11-6465-2011, 2011.

Novakov, T., Chang, S. G., and Harker, A. B.: Sulfates as pollution particulates: Catalytic formation on carbon (soot) particles, Science, 186, 259–261, https://doi.org/10.1126/science.186.4160.259, 1974.

Oberdüörster, G.: Toxicology of ultrafine particles: in vivo studies, Philosophical Transactions of the Royal Society of London A: Mathematical, Physical and Engineering Sciences, 358, 2719–2740, https://doi.org/10.1098/rsta.2000.0680, http://rsta.royalsocietypublishing.org/content/358/1775/2719, 2000.

Ortega, A. M., Hayes, P. L., Peng, Z., Palm, B. B., Hu, W. W., Day, D. A., Li, R., Cubison, M. J., Brune, W. H., Graus, M., Warneke, C., and Gilman, J. B.: Real-time measurements of secondary organic aerosol formation and aging from ambient air in an oxidation flow reactor in the Los Angeles area, Atmospheric Chemistry and Physics Discussions, 15, 7411–7433, https://doi.org/10.5194/acp-16-7411-2016, http://dx.doi.org/10.5194/acp-16-7411-2016, 2016.

Ovadnevaite, J., O'Dowd, C., Dall'Osto, M., Ceburnis, D., Worsnop, D. R., and Berresheim, H.: Detecting high contributions of primary organic matter to marine aerosol: A case study, Geophysical Research Letters, 38, 2–6, https://doi.org/10.1029/2010GL046083, 2011.

Paatero, P.: User's guide for positive matrix factorization programs PMF2.exe and PMF3.exe, University of Helsinki, Finland, 2007.

Paatero, P. and Tapper, U.: Positive matrix factorization: A non-negative factor model with optimal utilization of error estimates of data values, Environmetrics, 5, 111–126, https://doi.org/10.1002/env.3170050203, http://dx.doi.org/10.1002/env.3170050203, 1994.

Port of Oakland: Port of Oakland's largest terminal says night gates here to stay, Press Release, https://www.portofoakland.com/press-releases/port-oaklands-largest-terminal-says-night-gates-stay/, 2016.

Preble, C. V., Dallmann, T. R., Kreisberg, N. M., Hering, S. V., Harley, R. A., and Kirchstetter, T. W.: Effects of Particle Filters and Selective Catalytic Reduction on Heavy-Duty Diesel Drayage Truck Emissions at the Port of Oakland, Environmental Science and Technology, 49, 8864–8871, https://doi.org/10.1021/acs.est.5b01117, http://dx.doi.org/10.1021/acs.est.5b01117, 2015.

Preble, C. V., Cados, T. E., Harley, R. A., and Kirchstetter, T. W.: In-Use Performance and Durability of Particle Filters on Heavy-Duty Diesel Trucks, Environmental Science & Technology, 0, null, https://doi.org/10.1021/acs.est.8b02977, https://doi.org/10.1021/acs.est.8b02977, pMID: 30153019, 2018.

Presto, A. A., Gordon, T. D., and Robinson, A. L.: Primary to secondary organic aerosol: Evolution of organic emissions from mobile combustion sources, Atmospheric Chemistry and Physics, 14, 5015–5036, https://doi.org/10.5194/acp-14-5015-2014, 2014.

Robinson, A. L., Donahue, N. M., Shrivastava, M. K., Weitkamp, E. a., Sage, A. M., Grieshop, A. P., Lane, T. E., Pierce, J. R., and Pandis, S. N.: Rethinking organic aerosols: Semivolatile emissions and photochemical aging, Science, 315, 1259–1262, https://doi.org/10.1126/science.1133061, 2007.

Robinson, A. L., Grieshop, A. P., Donahue, N. M., and Hunt, S. W.: Updating the Conceptual Model for Fine Particle Mass Emissions from Combustion Systems Allen L. Robinson, Journal of the Air &Waste Management Association, 60, 1204–1222, , , 2010.

Robinson, E. S., Gu, P., Ye, Q., Li, Z., Shah, R. U., Apte, J. S., Robinson, A. L., and Presto, A. A.: Restaurant impacts on outdoor air quality: elevated organic aerosol mass from restaurant cooking with neighborhood-scale plume extents, Environmental Science & Technology, Submitted., 2018.

Saha, P. K., Khlystov, A., Snyder, M. G., and Grieshop, A. P.: Characterization of air pollutant concentrations, fleet emission factors, and dispersion near a North Carolina interstate freeway across two seasons, Atmospheric Environment, 177, 143–153, https://doi.org/10.1016/j.atmosenv.2018.01.019, https://doi.org/10.1016/j.atmosenv.2018.01.019, 2018a.

Saha, P. K., Khlystov, A., Snyder, M. G., and Grieshop, A. P.: Characterization of air pollutant concentrations, fleet emission factors, and dispersion near a North Carolina interstate freeway across two seasons, Atmospheric Environment, 177, 143–153, https://doi.org/10.1016/j.atmosenv.2018.01.019, https://doi.org/10.1016/j.atmosenv.2018.01.019, 2018b.

Saliba, G., Saleh, R., Zhao, Y., Presto, A. A., Lambe, A. T., Frodin, B., Sardar, S., Maldonado, H., Maddox, C., May, A. A., Drozd, G. T., Goldstein, A. H., Russell, L. M., Hagen, F., and Robinson, A. L.: Comparison of Gasoline Direct-Injection (GDI) and Port Fuel Injection

(PFI) Vehicle Emissions: Emission Certification Standards, Cold-Start, Secondary Organic Aerosol Formation Potential, and Potential Climate Impacts, Environmental Science and Technology, 51, 6542–6552, https://doi.org/10.1021/acs.est.6b06509, 2017.

Schmale, J., Schneider, J., Nemitz, E., Tang, Y. S., Dragosits, U., Blackall, T. D., Trathan, P. N., Phillips, G. J., Sutton, M., and Braban, C. F.: Sub-Antarctic marine aerosol: Dominant contributions from biogenic sources, Atmospheric Chemistry and Physics, 13, 8669–8694, https://doi.org/10.5194/acp-13-8669-2013, 2013.

Seinfeld, J. and Pandis, S. N.: Atmospheric Chemistry and Physics: From Air Pollution to Climate Change, chap. 21, Section 26.2, John Wiley and Sons, Inc., New York, 2 edn., 2006.

Stölzel, M., Breitner, S., Cyrys, J., Pitz, M., Wölke, G., Kreyling, W., Heinrich, J., Wichmann, H. E., and Peters, A.: Daily mortality and particulate matter in different size classes in Erfurt, Germany, Journal of Exposure Science and Environmental Epidemiology, 17, 458–467, https://doi.org/10.1038/sj.jes.7500538, http://dx.doi.org/10.1038/sj.jes.7500538, 2007.

Stutz, J., Kim, E. S., Platt, U., Bruno, P., Perrino, C., and Febo, A.: UV-visible absorption cross sections of nitrous acid, Journal of Geophysical Research Atmospheres, 105, 14 585–14 592, https://doi.org/10.1029/2000JD900003, https://www.scopus.com/inward/record.uri?eid=2-s2.0-0033793746{&}partnerID=40{&}md5=df56e17158e0b457ca4fe8693f776846, 2000.

Sueper, D., Allan, J. D., Dunlea, E., Crosier, J., Kimmel, J. R., DeCarlo, P. F., Aiken, A. C., and Jimenez, J. L.: A Community Software for Quality Control and Analysis of Data from the Aerodyne Time-of-Flight Aerosol Mass Spectrometers (ToF-AMS), Tech. rep., Reno, NV, 2007.

Sun, Y. L., Zhang, Q., Schwab, J. J., Demerjian, K. L., Chen, W. N., Bae, M. S., Hung, H. M., Hogrefe, O., Frank, B., Rattigan, O. V., and Lin, Y. C.: Characterization of the sources and processes of organic and inorganic aerosols in New York city with a high-resolution time-of-flight aerosol mass apectrometer, Atmospheric Chemistry and Physics, 11, 1581–1602, https://doi.org/10.5194/acp-11-1581-2011, http://dx.doi.org/10.5194/acp-11-1581-2011, 2011.

Tao, L., Fairley, D., Kleeman, M. J., and Harley, R. A.: Effects of switching to lower sulfur marine fuel oil on air quality in the San Francisco Bay area, Environmental Science and Technology, 47, 10 171–10 178, https://doi.org/10.1021/es401049x, http://dx.doi.org/10.1021/es401049x, 2013.

Tsigaridis, K., Krol, M., Dentener, F. J., Balkanski, Y., Lathière, J., Metzger, S., Hauglustaine, D. A., and Kanakidou, M.: Change in global aerosol composition since preindustrial times, Atmospheric Chemistry and Physics, 6, 5143–5162, https://doi.org/10.5194/acp-6-5143-2006, http://dx.doi.org/10.5194/acp-6-5143-2006, 2006.

Ulbrich, I. M., Canagaratna, M. R., Zhang, Q., Worsnop, D. R., and Jimenez, J. L.: Interpretation of Organic Components from Positive Matrix Factorization of Aerosol Mass Spectrometric Data., Atmos. Chem. Phys., 9, 2891, https://doi.org/10.5194/acp-9-2891-2009, http://dx.doi.org/10.5194/acp-9-2891-2009, 2009.

Ulbrich, I. M., Handschy, A., Lechner, M., and Jimenez, J. L.: High-Resolution AMS Spectral Database, http://cires1.colorado.edu/jimenez-group/HRAMSsd/, 2018.

United Nations: World Urbanization Prospects, Tech. rep., United Nations, Department of Economic and Social Affairs, https://doi.org/10.4054/DemRes.2005.12.9, http://dx.doi.org/10.4054/DemRes.2005.12.9, 2014.

US Census: US Census Bureau Reporter - Oakland, CA, https://censusreporter.org/profiles/16000US0653000-oakland-ca/, 2016.

Van den Bossche, J., Peters, J., Verwaeren, J., Botteldooren, D., Theunis, J., and De Baets, B.: Mobile monitoring for mapping spatial variation in urban air quality: Development and validation of a methodology based on an extensive dataset, Atmospheric Environment, 105, 148–161, https://doi.org/10.1016/j.atmosenv.2015.01.017, http://dx.doi.org/10.1016/j.atmosenv.2015.01.017, 2015.

Villena, G., Kleffmann, J., Kurtenbach, R., Wiesen, P., Lissi, E., Rubio, M. A., Croxatto, G., and Rappenglück, B.: Vertical gradients of HONO, NOx and O3 in Santiago de Chile, Atmospheric Environment, 45, 3867–3873, https://doi.org/10.1016/j.atmosenv.2011.01.073, http://dx.doi.org/10.1016/j.atmosenv.2011.01.073, 2011.

Von Der Weiden-Reinmüller, S. L., Drewnick, F., Zhang, Q. J., Freutel, F., Beekmann, M., and Borrmann, S.: Megacity emission plume characteristics in summer and winter investigated by mobile aerosol and trace gas measurements: The Paris metropolitan area, Atmospheric Chemistry and Physics, 14, 12 931–12 950, https://doi.org/10.5194/acp-14-12931-2014, ,-2014.

Worton, D. R., Isaacman, G., Gentner, D. R., Dallmann, T. R., Chan, A. W., Ruehl, C., Kirchstetter, T. W., Wilson, K. R., Harley, R. A., and Goldstein, A. H.: Lubricating oil dominates primary organic aerosol emissions from motor vehicles, Environmental Science and Technology, 48, 3698–3706, https://doi.org/10.1021/es405375j, 2014.

Xu, L., Suresh, S., Guo, H., Weber, R. J., and Ng, N. L.: Aerosol characterization over the southeastern United States using high-resolution aerosol mass spectrometry: Spatial and seasonal variation of aerosol composition and sources with a focus on organic nitrates, Atmospheric Chemistry and Physics, 15, 7307–7336, https://doi.org/10.5194/acp-15-7307-2015, 2015.

Ye, Q., Gu, P., Li, H. Z., Robinson, E. S., Lipsky, E., Kaltsonoudis, C., Lee, A. K., Apte, J. S., Robinson, A. L., Sullivan, R. C., Presto, A. A., and Donahue, N. M.: Spatial Variability of Sources and Mixing State of Atmospheric Particles in a Metropolitan Area, Environmental Science & Technology, 0, null, https://doi.org/10.1021/acs.est.8b01011, https://doi.org/10.1021/acs.est.8b01011, pMID: 29775536, 2018.

Yuan, C., Ng, E., and Norford, L. K.: Improving air quality in high-density cities by understanding the relationship between air pollutant dispersion and urban morphologies, Building and Environment, 71, 245–258, https://doi.org/10.1016/j.buildenv.2013.10.008, http://dx.doi.org/10.1016/j.buildenv.2013.10.008, 2014.

Yun, H., Wang, Z., Zha, Q., Wang, W., Xue, L., Zhang, L., Li, Q., Cui, L., Lee, S., Poon, S. C., and Wang, T.: Nitrous acid in a street canyon environment: Sources and contributions to local oxidation capacity, Atmospheric Environment, 167, 223–234, https://doi.org/10.1016/j.atmosenv.2017.08.018, http://dx.doi.org/10.1016/j.atmosenv.2017.08.018, 2017.

Zhang, Q., Jimenez, J. L., Canagaratna, M. R., Allan, J. D., Coe, H., Ulbrich, I., Alfarra, M. R., Takami, A., Middlebrook, A. M., Sun, Y. L., Dzepina, K., Dunlea, E., Docherty, K., DeCarlo, P. F., Salcedo, D., Onasch, T., Jayne, J. T., Miyoshi, T., Shimono, A., Hatakeyama, S., Takegawa, N., Kondo, Y., Schneider, J., Drewnick, F., Borrmann, S., Weimer, S., Demerjian, K., Williams, P., Bower, K., Bahreini, R., Cottrell, L., Griffin, R. J., Rautiainen, J., Sun, J. Y., Zhang, Y. M., and Worsnop, D. R.: Ubiquity and dominance of oxygenated species in organic aerosols in anthropogenically-influenced Northern Hemisphere midlatitudes, Geophysical Research Letters, 34, 1–6, https://doi.org/10.1029/2007GL029979, http://dx.doi.org/10.1029/2007GL029979, 2007.

Zhang, Q., Jimenez, J. L., Canagaratna, M. R., Ulbrich, I. M., Ng, N. L., Worsnop, D. R., and Sun, Y.: Understanding atmospheric organic aerosols via factor analysis of aerosol mass spectrometry: A review, Analytical and Bioanalytical Chemistry, 401, 3045–3067, https://doi.org/10.1007/s00216-011-5355-y, http://dx.doi.org/10.1007/s00216-011-5355-y, 2011.

Zhao, Y., Nguyen, N. T., Presto, A. A., Hennigan, C. J., May, A. A., and Robinson, A. L.: Intermediate Volatility Organic Compound Emissions from On-Road Diesel Vehicles: Chemical Composition, Emission Factors, and Estimated Secondary Organic Aerosol Production, Environmental Science and Technology, 49, 11 516–11 526, https://doi.org/10.1021/acs.est.5b02841, 2015.

Zhong, J., Cai, X. M., and Bloss, W. J.: Large eddy simulation of reactive pollutants in a deep urban street canyon: Coupling dynamics with O3-NOx-VOC chemistry, Environmental Pollution, 224, 171–184, https://doi.org/10.1016/j.envpol.2017.01.076, http://dx.doi.org/10.1016/j.envpol.2017.01.076, 2017.

Zimmerman, N., Li, H. Z., Ellis, A. A., Hauryliuk, A., Robinson, E. S., Gu, P., Shah, R. U., Ye, Q., Snell, L., R., S., Robinson, A. L., Apte, J. S., and Presto, A. A.: Integrating Spatiotemporal Variability and Modifiable Factors into Air Pollution Estimates: The Center for Air, Climate, and Energy Solutions Air Quality Observatory, Atmospheric Environment, Submitted, 2018.

Supplemental information for

High spatial resolution mapping of aerosol composition and sources in Oakland, California using mobile aerosol mass spectrometry

Shah et al.

Correspondence to: Albert A. Presto (apresto@andrew.cmu.edu)

A1 Accounting for temporal trends

Over the course of mobile sampling, the urban background air quality can have daily and diurnal variations due to meteorological changes. These variations can be accounted for with the help of concurrent stationary measurements performed at an urban background location, provided this background location is not in close proximity ($\leq$ 50 m) of a major emission source (e.g., a street with > 3000 daily vehicles, construction sites, industrial emissions, etc; Hoek et al., 2002; Van den Bossche et al., 2015). Further, different meteorological conditions (temperature, relative humidity, solar irradiation) influence individual components of particulate matter differently (e.g., the gas-particle partitioning of NO_3^-, SO_4^{2-} and OA have different sensitivities to temperature; more irradiation can indirectly result in more secondary OA). Ideally, the temporal correction of mobile measurements of a particular PM component would be performed using background measurements of that individual component performed in the same manner. Thus, mobile AMS measurements should ideally be corrected using concurrent stationary AMS measurements (Mohr et al., 2015).

We did not perform concurrent stationary AMS measurements in Oakland in this campaign. Stationary measurements of criteria pollutants (CO, NO_x, $PM_{2.5}$, etc.) were made by a regulatory monitor operated by the Bay Area air quality management district. However, this monitor was located in a parking lot within $\sim$ 30 m of a major street (> 20,000 vehicles daily; Knoderer et al., 2016). Due to this, we did not use this monitor as an indicator of diurnal variations in urban background. Instead, we assumed that by shuffling the order of visiting each polygon within the sampling domain, repeated measurements at a given point in space were well-balanced in time. We validated this assumption by running the timestamps of our data through the spatial aggregation routine described earlier. The resulting map (Figure S1) confirms that the measurements in this study were indeed well-balanced in space and time. Further, diurnal variations in meteorological factors had a consistent pattern on all days of this campaign (Figure S2), hence by balancing our samples in space and time, we assume that the effects of diurnal variations in urban background are nullified upon aggregation of data from multiple days.

Figure S2 shows that daily variations in meteorological factors is typically larger and sporadic relative to diurnal variations. To account for the possible effect of these daily variations on urban background, we tested a daily multiplicative correction factor to our mobile measurements based on stationary measurements of $PM_{2.5}$ at the regulatory site.

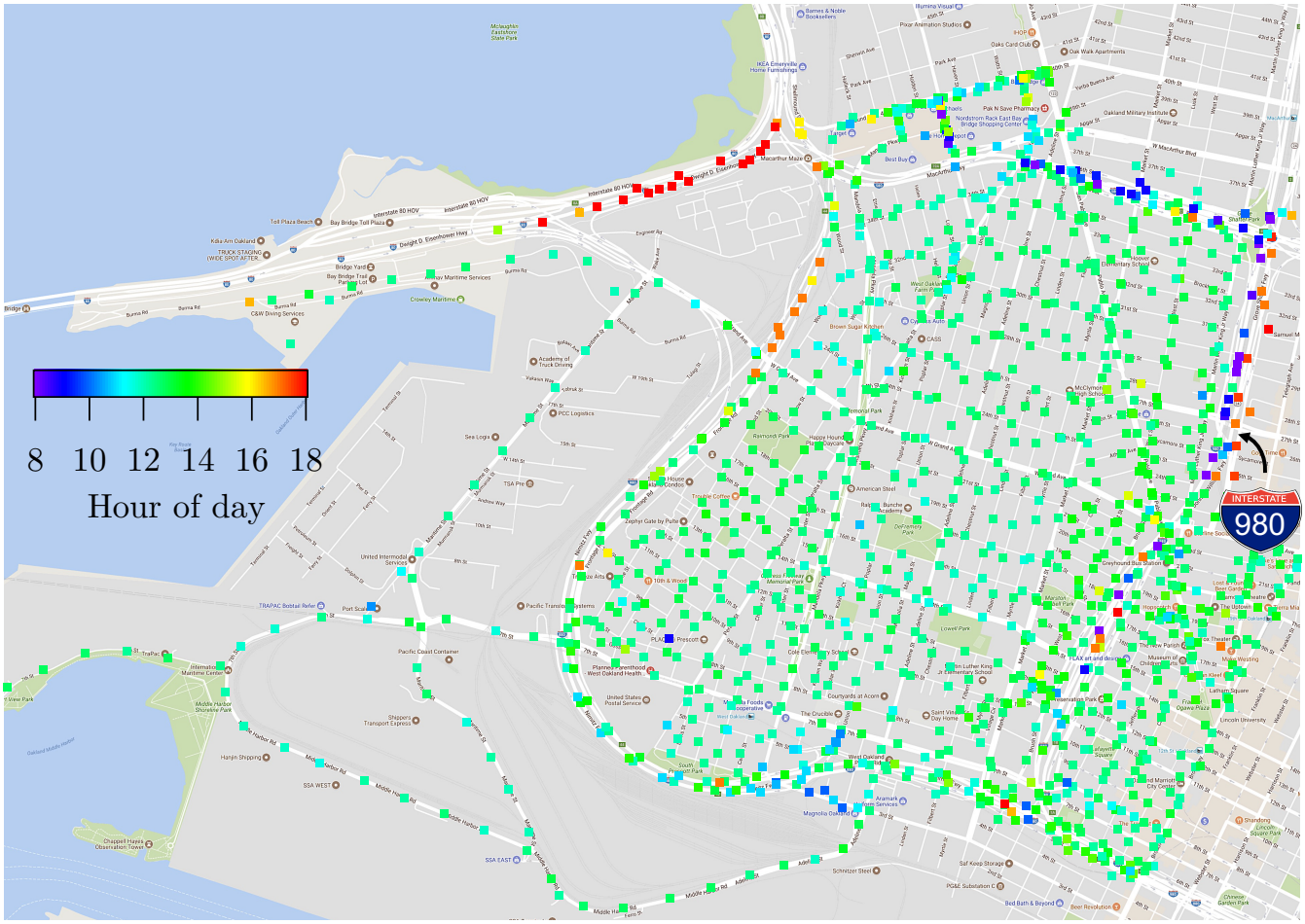

Figure S1. Spatially aggregated timestamp of all AMS measurements. Typically, drives were performed from 0800 to 1800 hours. If all parts of the domain were sampled randomly everyday, the average of all measurement timestamps should ideally occur at 1300 hours. This figure shows that this ideality was indeed realized in this campaign and that we balanced our measurements in space and time reasonably well. On most days, we used the south- and north-bound lanes of Interstate 980 to enter and exit the domain at 0800 and 1800 hours, respectively. As a result, there is a temporal bias in sampling this highway, as shown by the figure.

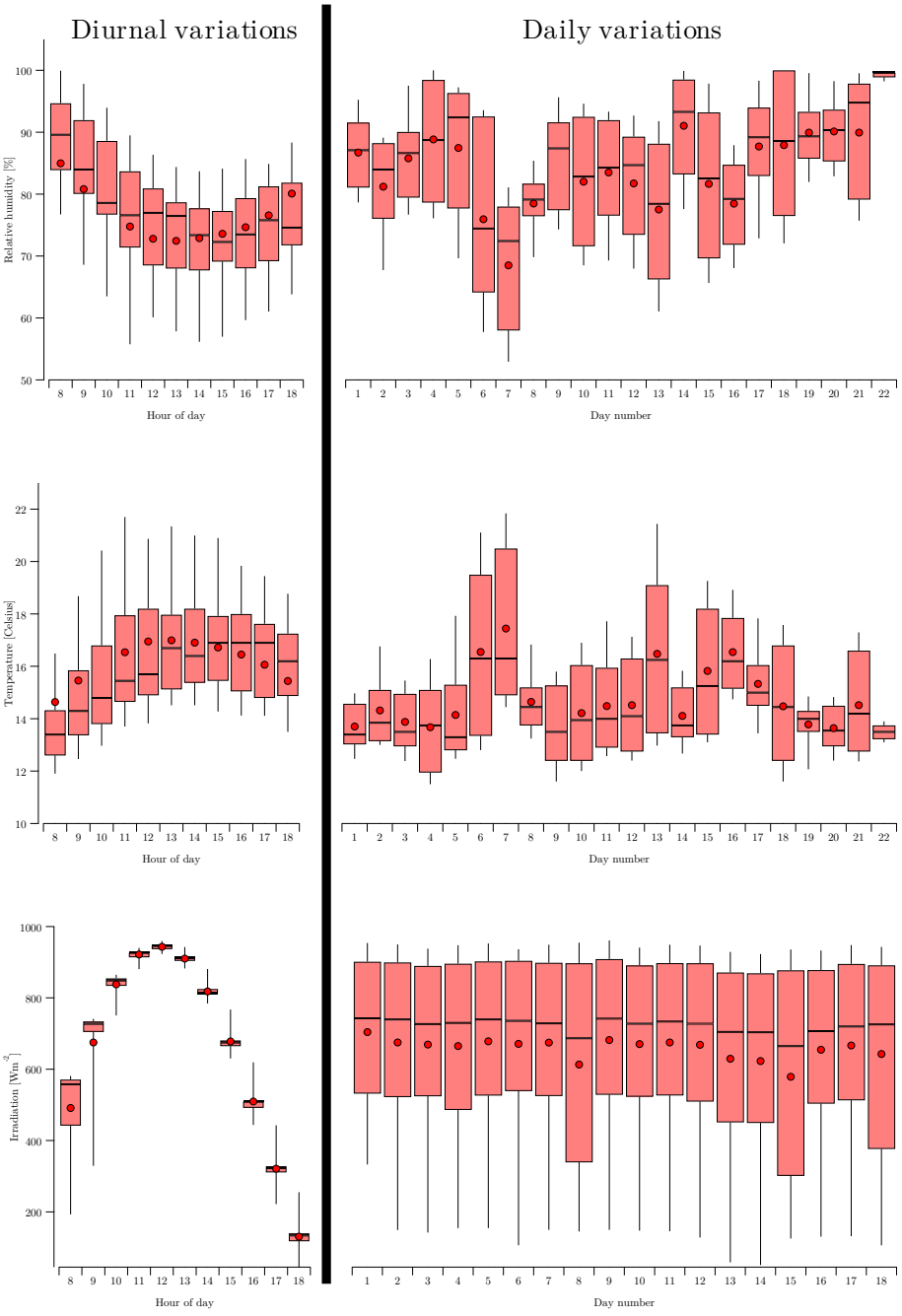

Figure S2. Diurnal and daily variations in meteorological factors in Oakland during the sampling period. Diurnal variations have a consistent pattern that repeats everyday. By comparison, daily variations have more sporadic variations.

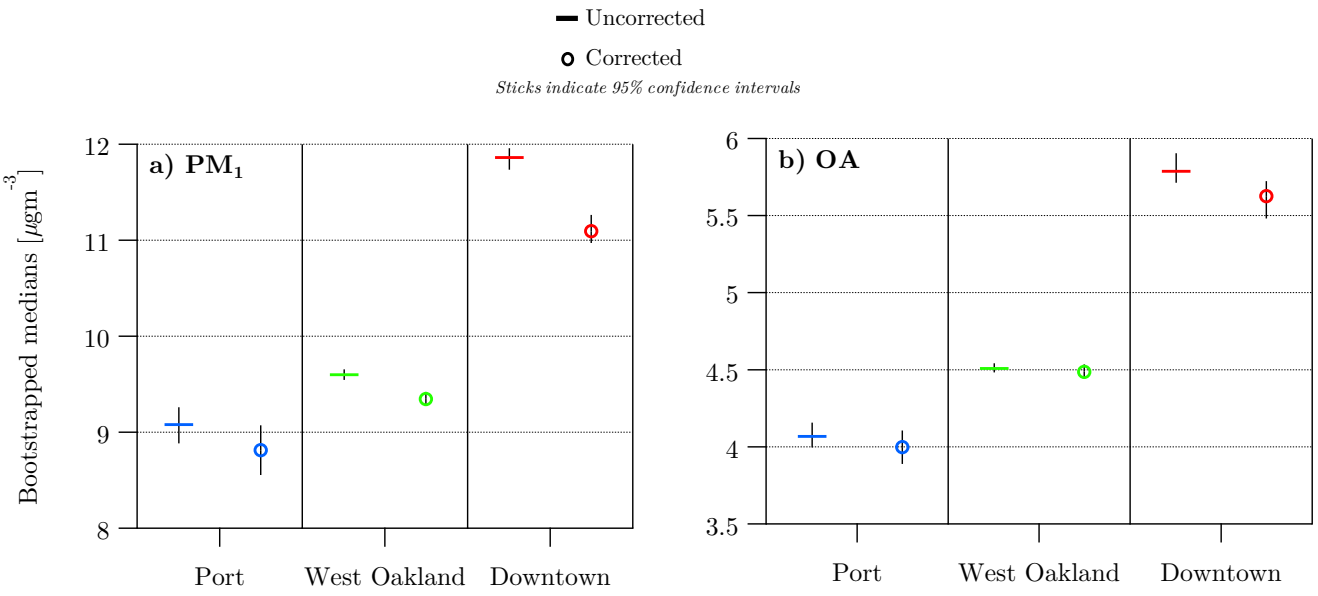

Figure S3. Effect of applying a daily correction factor to mobile measurements of a) PM_1 and b) OA. The 95% confidence intervals are achieved from bootstrapping and represent the difference between the 5th and 95th percentiles of the bootstrapped medians. Each day's correction factor is calculated as $CF_i = \frac{C_i}{C_{campaign}}$, where C_i is the median $PM_{2.5}$ concentration measured on the i^{th} day of the campaign, and $C_{campaign}$ is the median $PM_{2.5}$ concentration measured on all days of the campaign. Stationary $PM_{2.5}$ measurements were made by the regulatory monitor in West Oakland (Knoderer et al., 2016). Since we typically drove everyday from 8 AM to 6 PM, we only used stationary data from this daily time period.

A2 Sampling coverage

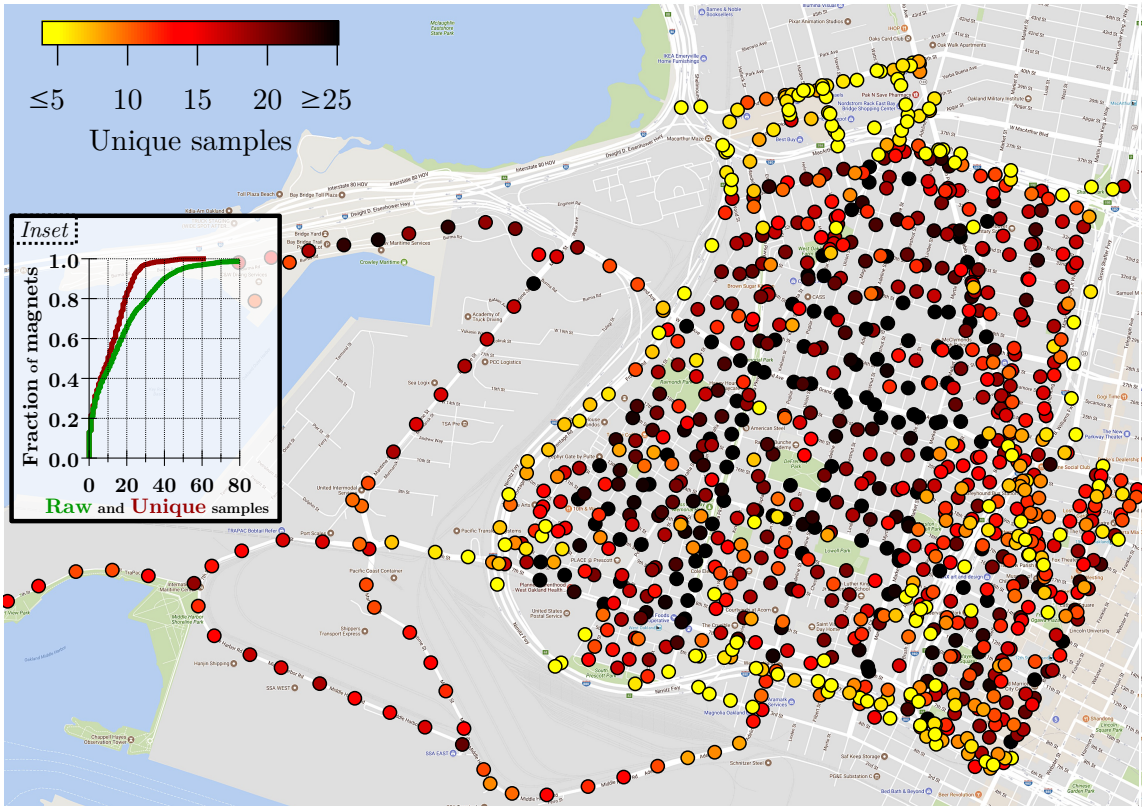

Figure S4. Sampling coverage of the domain. Inset: Cumulative distribution of raw and unique samples in all magnets in domain.

A3 Bootstrapping analysis

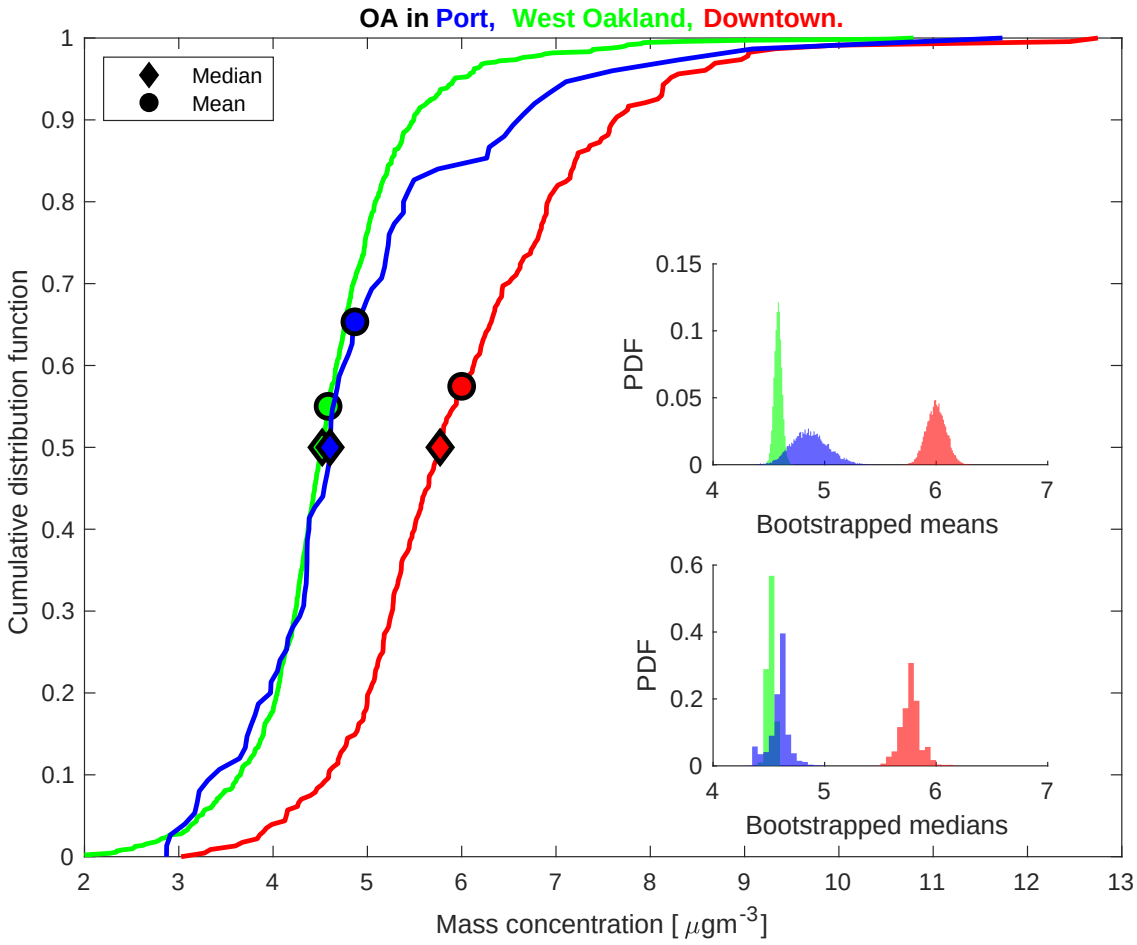

Figure S5. Polygon-specific cumulative distribution function (CDF) curves of spatially-aggregated OA concentrations. *Insets:* Probability distribution function (PDF) histograms for central tendency statistics (mean and median) of synthetic datasets created using bootstrap resampling. The PDF histogram for bootstrapped medians is shown with a coarser bin-width to guide the eye better. The abscissae on the insets have the same units as the parent abscissa, but with a zoomed-in scale.

~~Polygon-specific cumulative distribution function (CDF) curves of black carbon (BC) concentrations. *Insets:* Probability distribution function (PDF) histograms for central tendency statistics (mean and median) of synthetic datasets created using bootstrap resampling of raw data. The PDF histograms are shown with a coarser bin-width to guide the eye better. The abscissae on the insets have the same units as the parent abscissa, but with a zoomed-in scale.~~

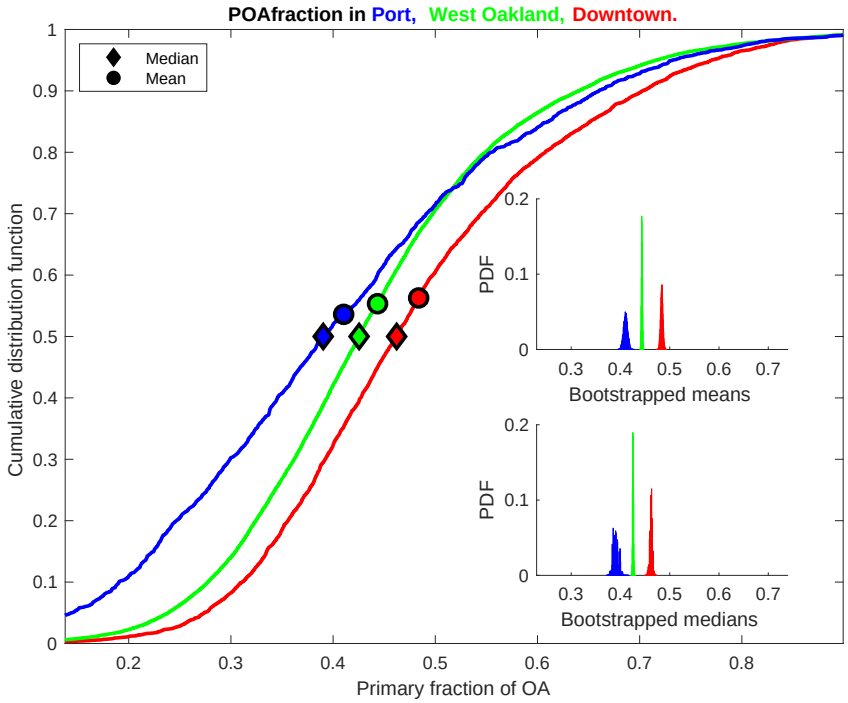

Figure S6. Cumulative distribution functions of primary fraction of OA (i.e., COA + HOA), resolved by area. Insets are results of bootstrapping.

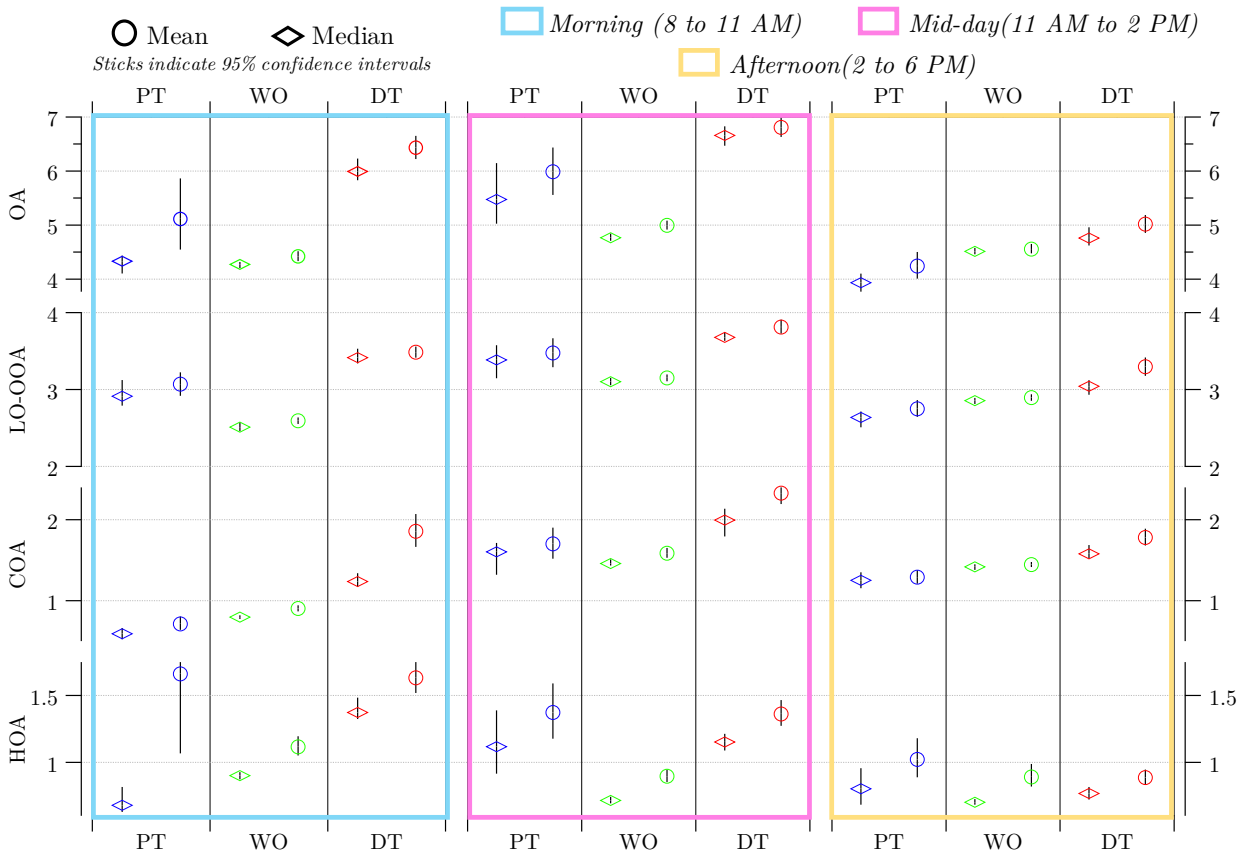

Figure S7. Bootstrapped statistics of OA and its factors, resolved by area and by time periods.

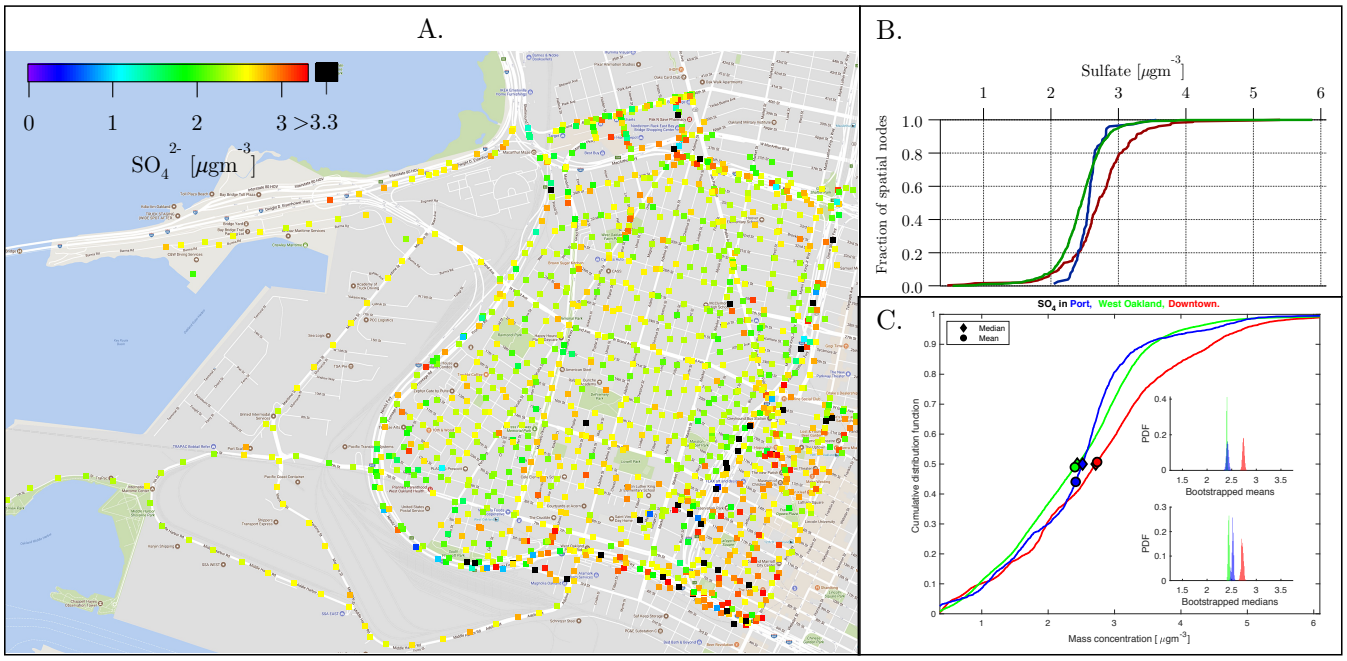

Figure S8. A: Median SO_4^{2-} at all magnets. **B:** Cumulative distribution function (CDF) curves of spatially-aggregated SO_4^{2-} concentrations. **C:** CDF curves of SO_4^{2-} concentrations without spatial aggregation. *Insets:* Probability distribution function (PDF) histograms for central tendency statistics (mean and median) of synthetic datasets created using bootstrap resampling of raw data. The abscissae on the insets have the same units as the parent abscissa, but with a zoomed-in scale.

It is seen that the CDFs of all polygons become “tighter" after spatial aggregation, which is expected, since the spatial aggregation routine reduces the spread in measurements via data reduction. However, the evidence of downtown being having a higher median (and especially higher mean) SO_4^{2-} than Port and West Oakland is not diminished by this data reduction, confirming that this trend is consistent across all days of sampling. Further, the SO_4^{2-} data exhibit minor positive skewness, suggesting that there are no local point sources of SO_4^{2-} in the domain.

A4 Quality of PMF solution

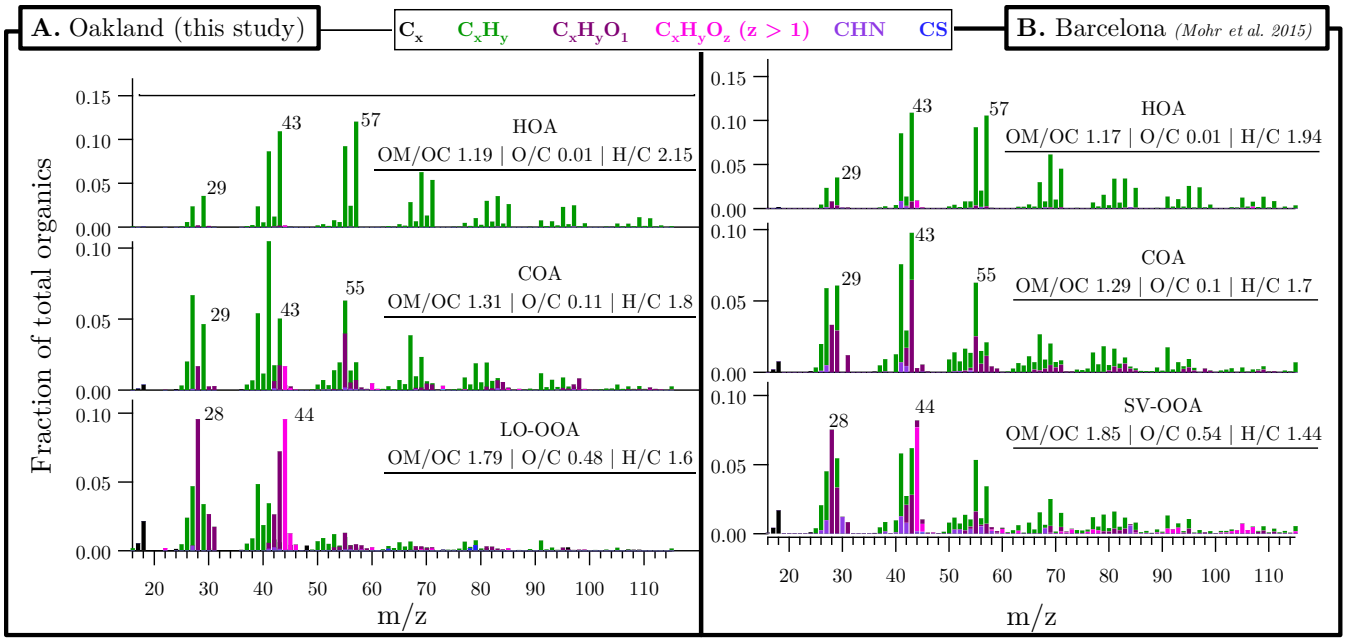

Figure S9. PMF factor mass spectra identified in **A.** Oakland and **B.** Barcelona (Mohr et al., 2015). Barcelona spectra obtained from the online high-resolution spectral database (Ulbrich et al., 2018, 2009).

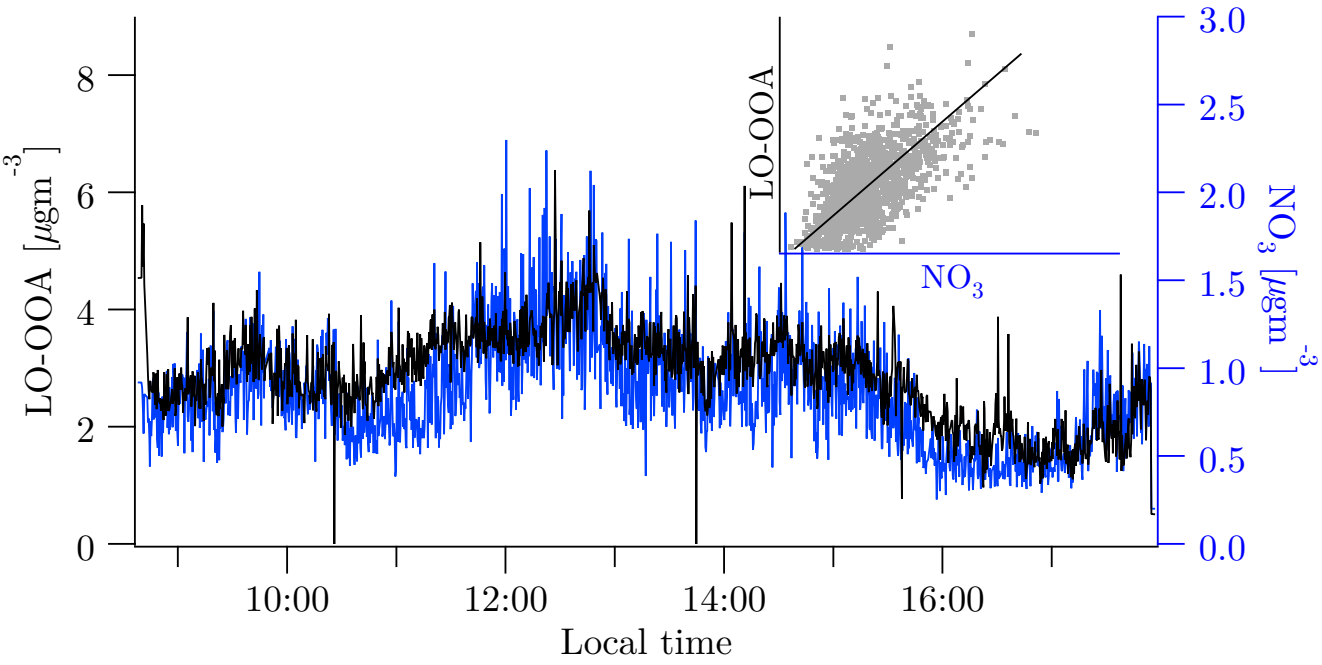

Figure S10. ~~SV-OOA~~ LO-OOA factor time series matched against NO_3^-, a marker for semi-volatile photochemically aged OA.

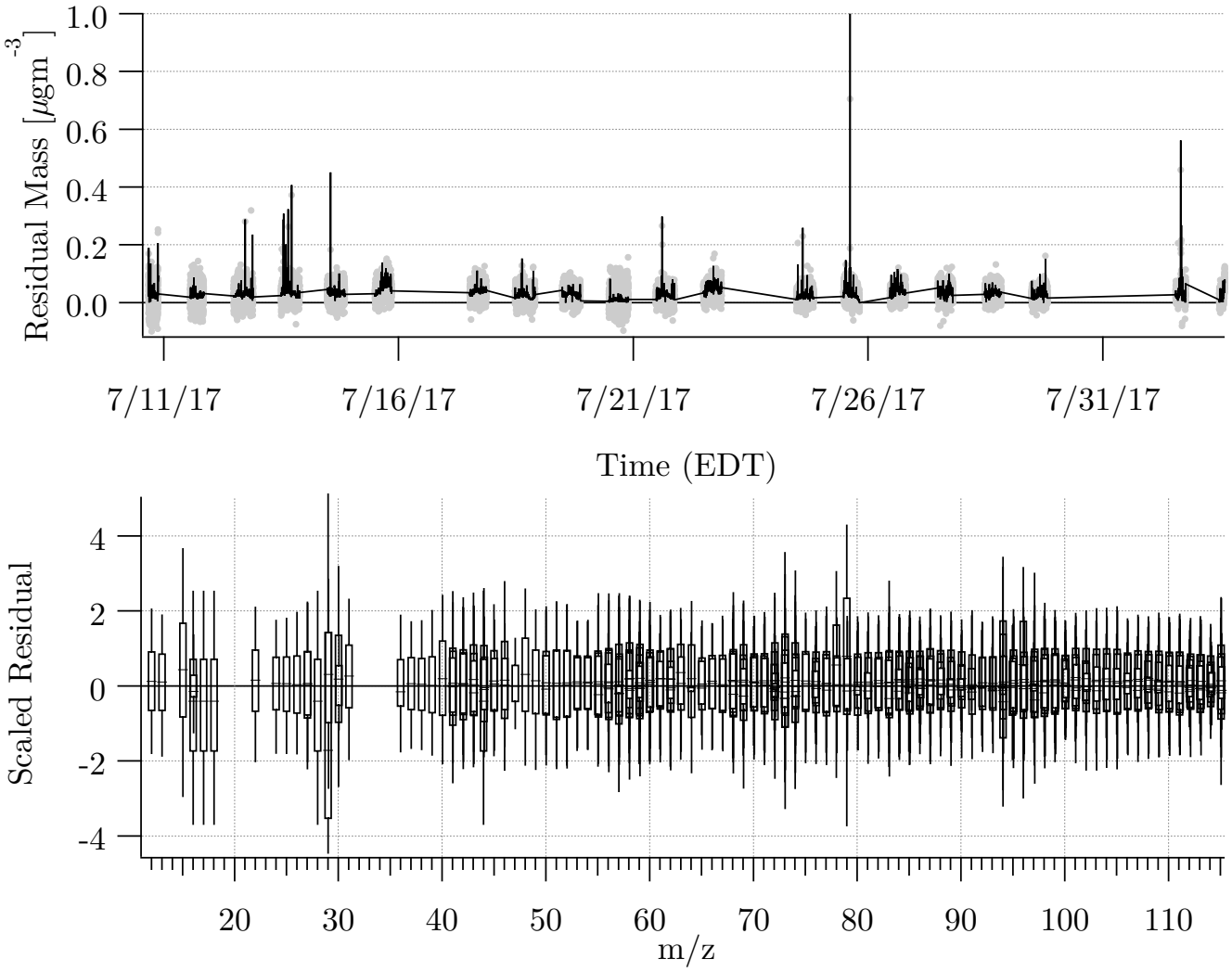

Figure S11. Residuals of three-factor PMF solution. The boxplots show the median (centerline) and quartiles (box limits) of the scaled residuals.

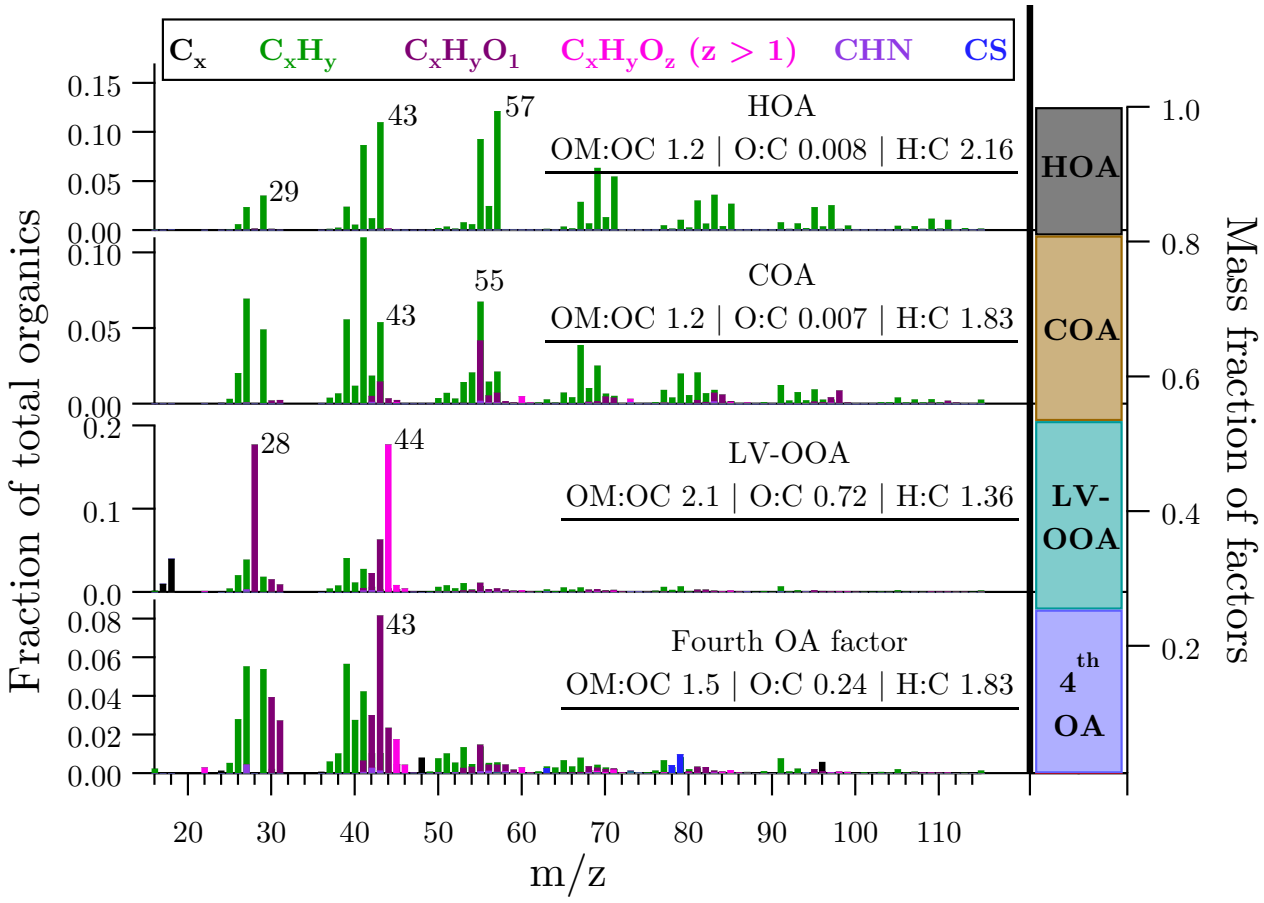

Figure S12. Mass spectra and elemental ratios of the four factors obtained from PMF analysis

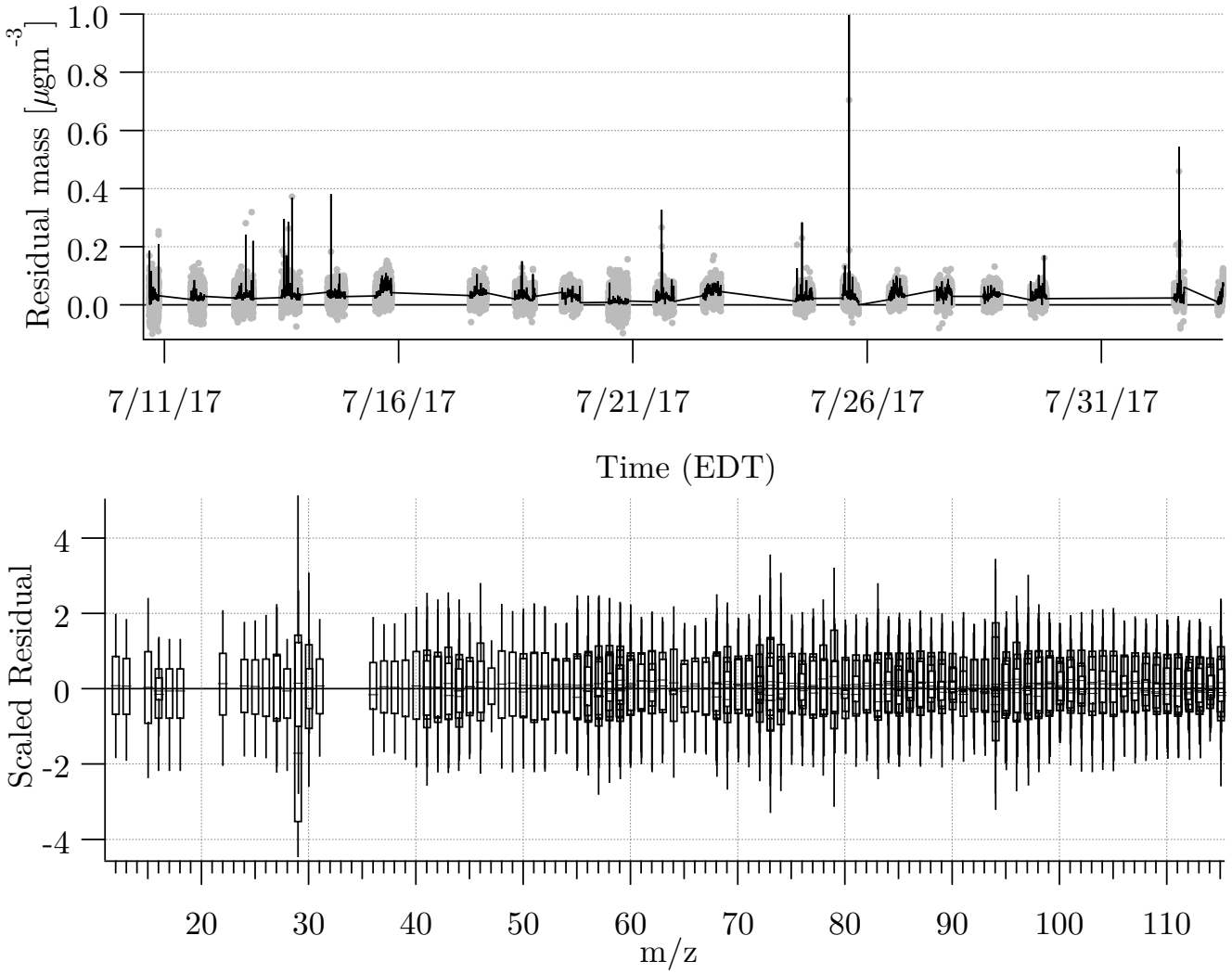

Figure S13. Residuals of four-factor PMF solution. The boxplots show the median (centerline) and quartiles (box limits) of the scaled residuals.

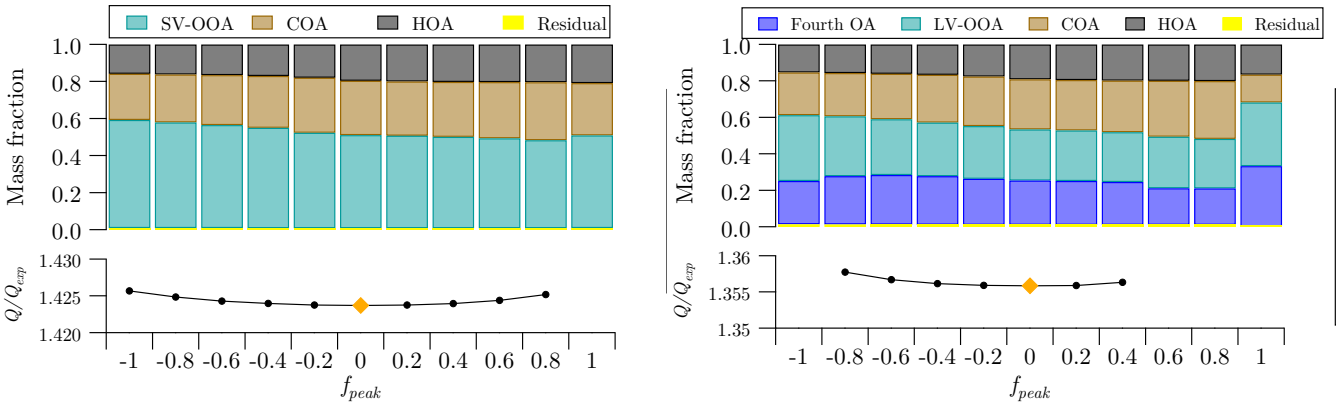

Figure S14. Variation in Q/Q_{exp} and mass fractions of factors with f_{peak} for 3- and 4-factor solutions. Q = sum of square of scaled residuals. Q_{exp} = number of degrees of freedom of the fitted data. Q/Q_{exp} should be ≈ 1. f_{peak} is a rotational parameter that can be chosen to examine different possible variations within an n-factor solution (Ulbrich et al., 2009).

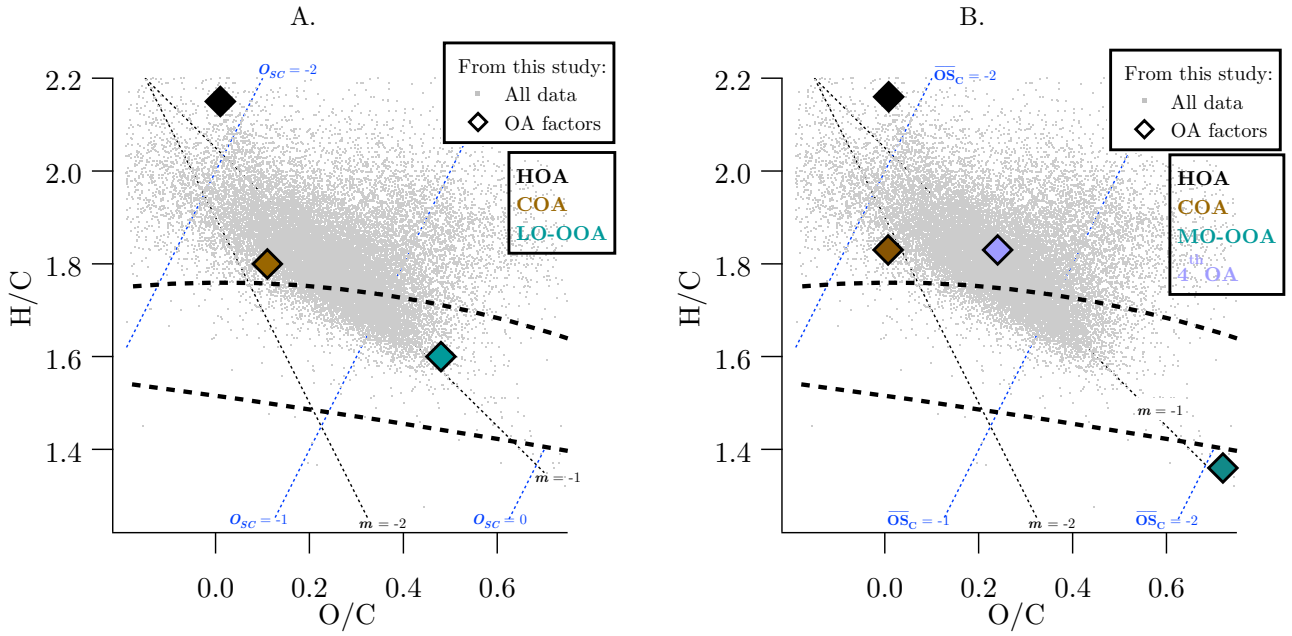

Figure S15. The Van Krevelen plane. Gray points represent all OA measurements in this study. Diamonds represent OA factors identified in the 3-factor (**A.**) and 4-factor (**B.**) PMF solution. Different oxygenation pathways are shown by the black dotted lines. Dotted blue lines are isopleths for average carbon oxidation states ($\overline{\text{OS}}_{\text{C}} = 2\times\text{O/C} - \text{H/C}$). The region of ambient oxygenated OA measurements, as reported by Ng et al. (2011) is shown between the dashed curves.

Marine influence.

Marine influence on aerosol properties has been shown to be important in some locations. For instance, Schmale et al. (2013) reported a "MSA-OA (methanesulfonic acid OA)" factor in their study on a remote island in the Antarctic ocean. By correlating particulate sulfate with this MSA mass contribution, Schmale et al. (2013) indeed show that marine influence on aerosol properties can be important (Figure S16A). We do not observe this marine influence in our data. Multiple lines of evidence point to this assessment: a) the correlation between particulate sulfate and MSA in Oakland (our data; Figure S16B) is $R^2 = 0.12$, while that of Schmale et al. (2013) is $R^2 = 0.72$, b) the ratio of MSA/sulfate in Oakland is only ~ 0.01, while that reported by Schmale et al. (2013) is ~ 0.25, c) the relative contribution of this MSA factor to the total OA in Oakland is less than 1% while that reported by Schmale et al. (2013) is 25%. That Oakland is an urban area and the measurement location of Schmale et al. (2013) was a remote island in the Antarctic explains these differences between the two datasets. Similarly, the work of Ovadnevaite et al. (2011) reported measurements in a remote location in Mace Head, Ireland which had a significant influence from marine OA with minor urban sources.

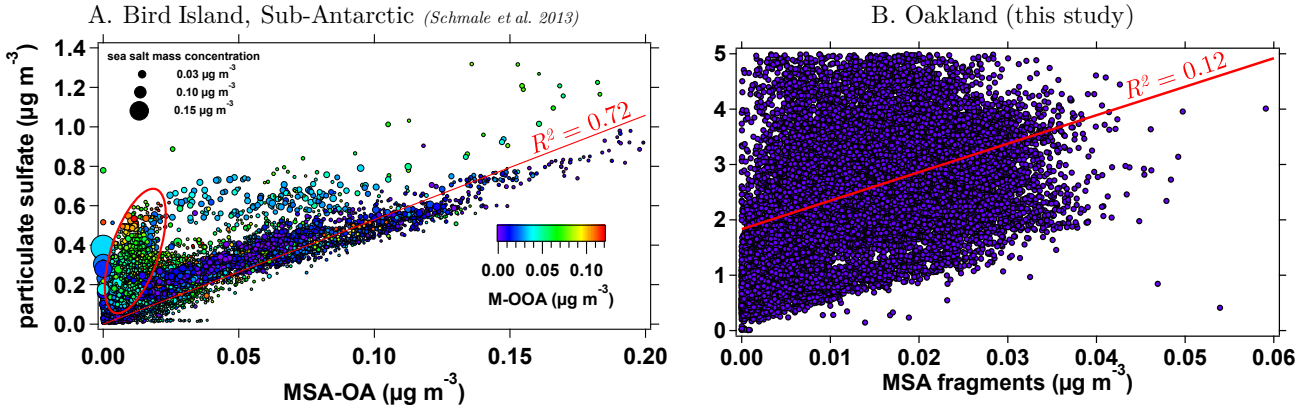

Figure S16. Correlation between particulate sulfate and methanesulfonic acid (MSA) OA reported in A) remote location of Bird Island research station in the sub-Antarctic region by Schmale et al. (2013) and B) Oakland (this study). Note: the axes on the two subplots are scaled differently. In the linear fit in the left subplot, Schmale et al. (2013) excluded data with M-OOA > 0.01 μgm^{-3} (e.g., data cluster in the ellipse), where M-OOA was a highly oxygenated PMF factor (O/C > 1), attributed to background wind trajectories.

Contrasting to these two studies in remote locations, Crippa et al. (2013a) and Mohr et al. (2015) performed measurements in urban areas and their PMF results showed urban OA factors (HOA, COA, SV-OOA). Similar to our results from Oakland, Mohr et al. (2015) revealed no marine OA influence in Barcelona, despite it being a coastal location and receiving sea breezes. On the other hand, Crippa et al. (2013a) reported a marine factor in Paris. Paris receives influence from different directions (urban as well as clean marine wind masses). Due to these very different static contributions to the total OA, the PMF analysis of Crippa et al. (2013a) was able to identify a distinct marine factor. However, in the case of Oakland, we are unable to mathematically show a distinct marine factor presence because the wind directions remain relatively stable. As a result, rather

than identify a distinct marine factor, PMF performs what is likely an artificial splitting, as explained previously in this section.

A5 Wind measurements

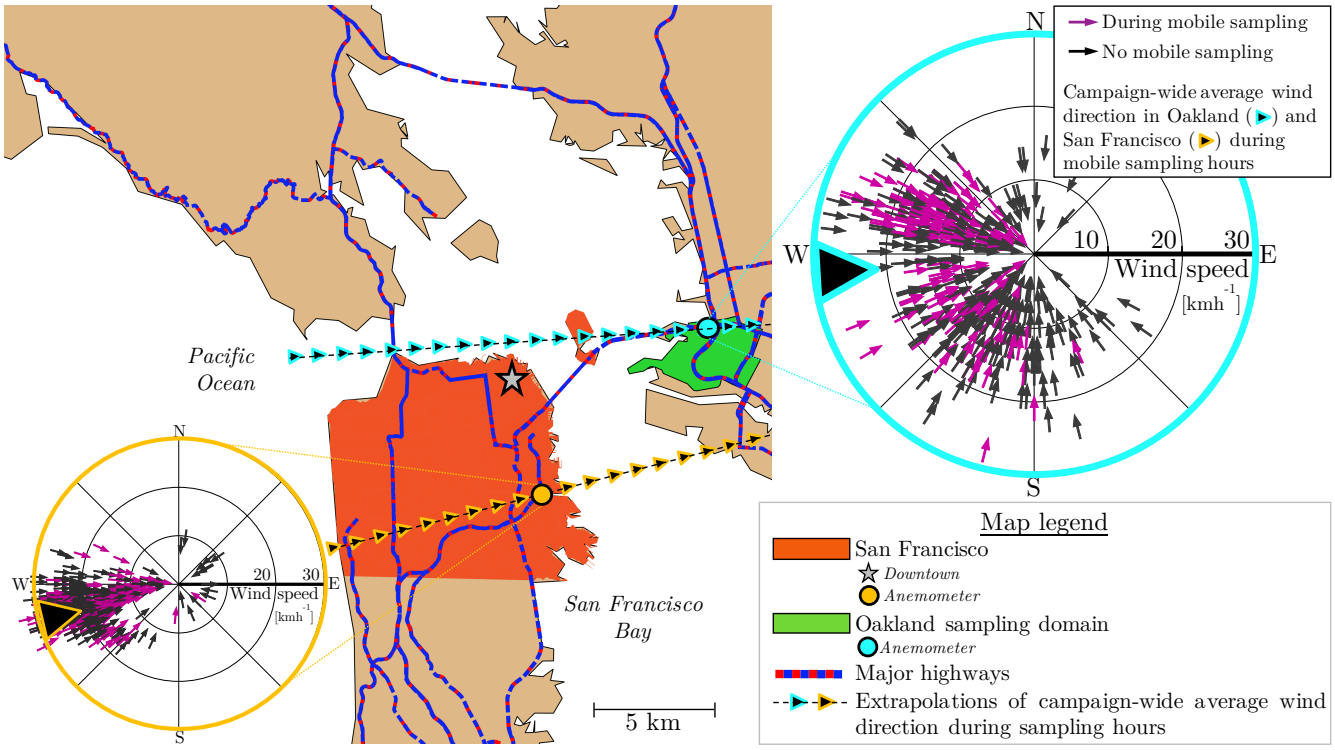

Figure S17. A map of the San Francisco (SF) Bay area, showing the location of the sampling domain in Oakland relative to SF city and downtown. Wind rose plots show hourly median wind speed and direction measured at two stationary anemometers in Oakland and San Francisco (BAAQMD, 2018). Purple wind rose arrows are wind measurements acquired during periods of concurrent mobile sampling (typically 8 am to 6 pm), while black arrows are measurements from when mobile sampling was not performed. A campaign-wide average of wind directions during periods of concurrent mobile sampling is shown by the triangle marker on each wind rose plot. The dashed lines with triangle markers are linear extrapolations of these campaign-wide average wind directions and are meant to guide the eye towards the regions over which these winds travel.

A6 OA factor maps

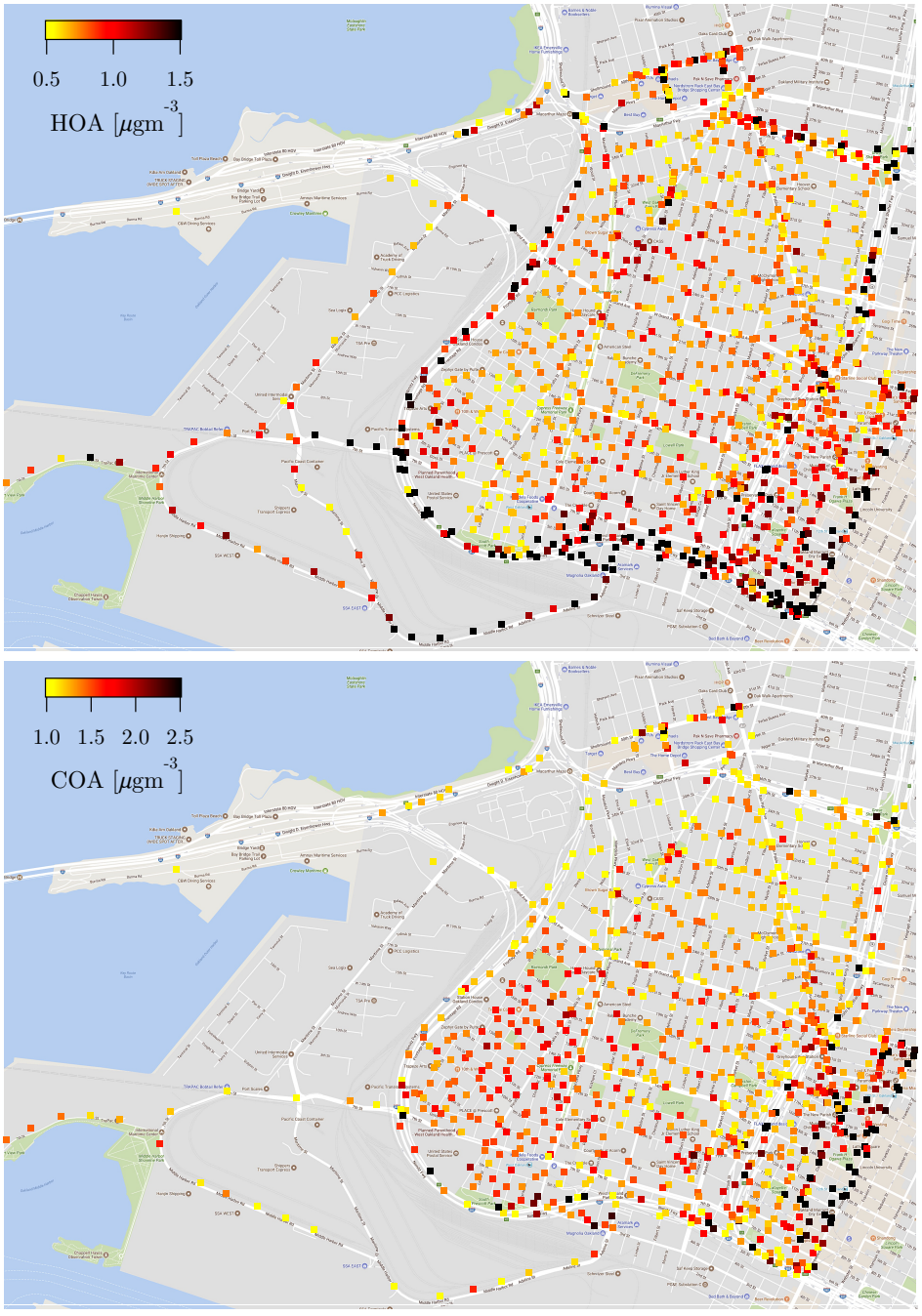

Figure S18. Maps of COA and HOA concentrations.

A7 Street canyon formation in downtown Oakland

Figure S19. Building height data for downtown polygon, obtained from City of Oakland (City of Oakland, 2017). The dashed black border shows limits of the downtown domain used in this study.

A8 Black carbon and CO maps

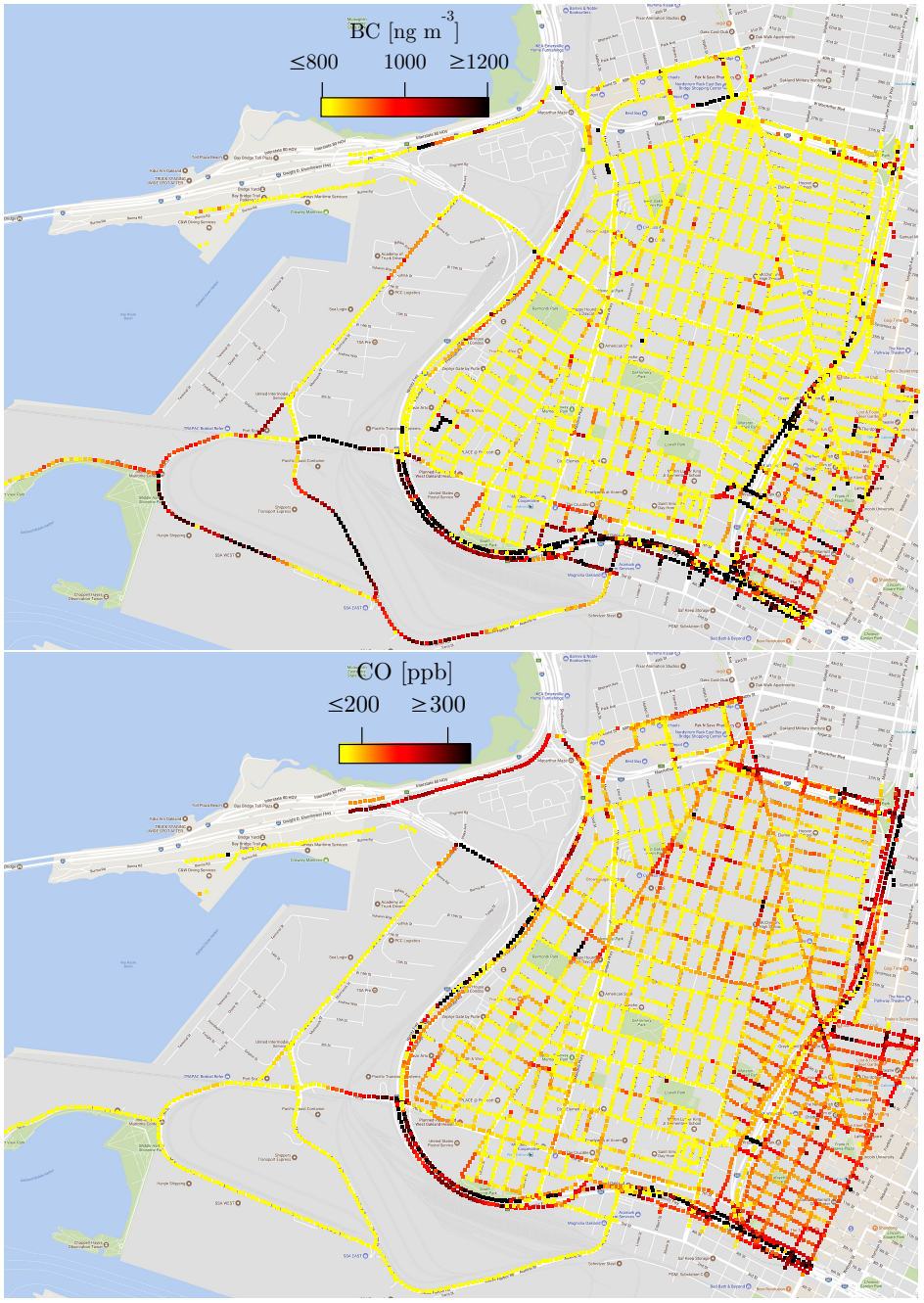

Figure S20. Black carbon and CO maps.

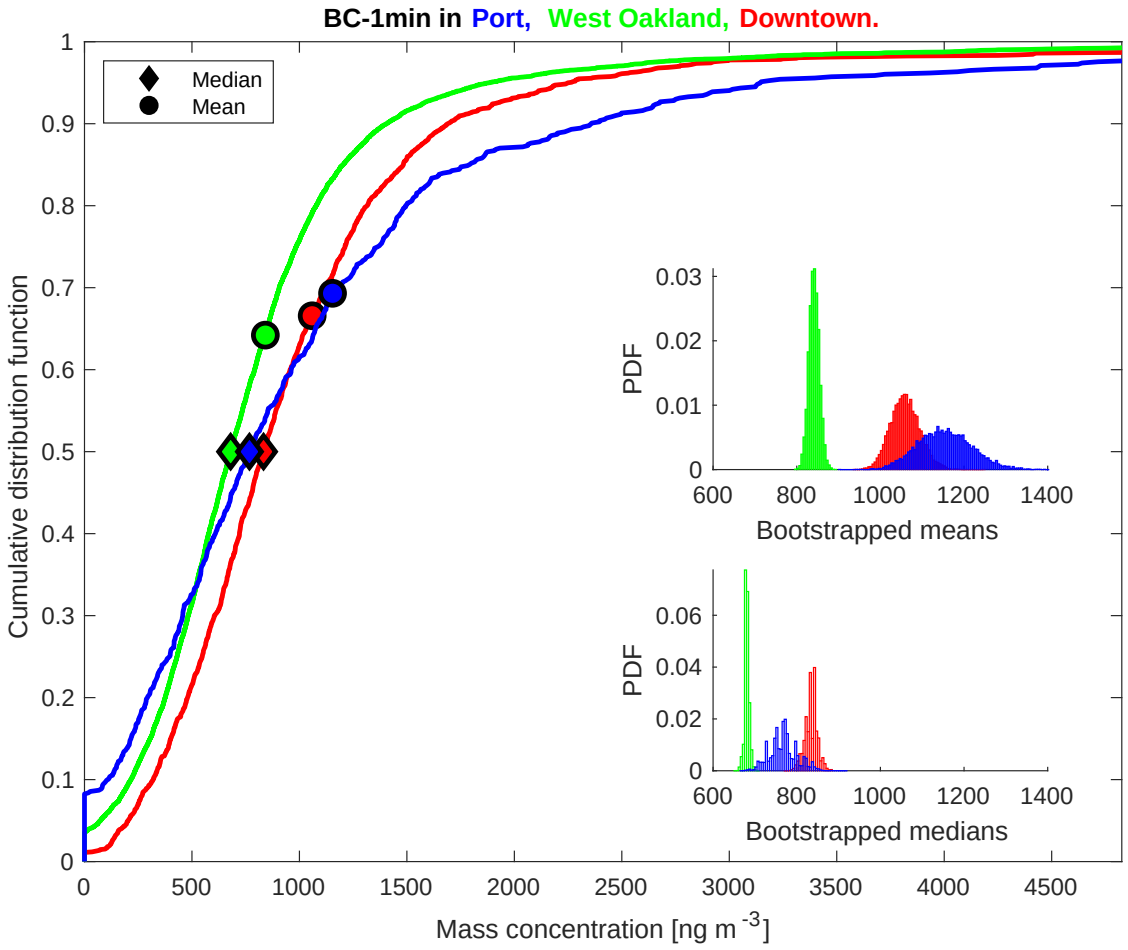

Figure S21. Polygon-specific cumulative distribution function (CDF) curves of black carbon (BC) concentrations. *Insets:* Probability distribution function (PDF) histograms for central tendency statistics (mean and median) of synthetic datasets created using bootstrap resampling of raw data. The PDF histograms are shown with a coarser bin-width to guide the eye better. The abscissae on the insets have the same units as the parent abscissa, but with a zoomed-in scale.